

~~SECRET~~  
**CONF-4**

# THE UNIVERSITY OF MICHIGAN

**COLLEGE OF ENGINEERING**  
**DEPARTMENT OF ELECTRICAL ENGINEERING**  
Radiation Laboratory

## INVESTIGATION OF RE-ENTRY VEHICLE SURFACE FIELDS (U)

QUARTERLY REPORT NO. 2

18 March 1966 - 18 June 1966

7741-2-Q = RL-2162

by

R. F. Goodrich, B. A. Harrison, E. F. Knott and V. H. Weston

June 1966

Contract AF 04(694)-834

Major A. Aharonian, Contract Monitor

In addition to security requirements which apply to this document and must be met, this document is subject to special export controls and each transmittal to foreign governments or foreign nationals may be made only with prior approval of BSD (ASSTT), Norton AFB, Calif., 92409.



**Contract With:** Ballistic Systems Division  
Deputy for Ballistic Missile Re-entry Systems  
Air Force Systems Command  
Norton AFB, California

~~SECRET~~

**Administered through:** **CONF-4**  
**OFFICE OF RESEARCH ADMINISTRATION · ANN ARBOR**

~~DOD DIRECTIVE CATEGORY 4~~  
~~DOWNGRADED AT 3-YEAR~~  
~~INTERVALS. DOWNGRADED TO~~  
~~UNCLASSIFIED AFTER 12 YEARS~~

~~This document contains information affecting the national defense of the United States within the meaning of the Espionage Laws, Title 18 U. S. C., sections 793 and 794, its transmission or the revelation of its contents in any manner to an unauthorized person is prohibited by law.~~

**SECRET**

7741-2-Q

BSD TR 66-255

Investigation of Re-entry Vehicle Surface Fields (U)

Quarterly Report No. 2

18 March 1966 - 18 June 1966

AF 04(694)-834

by

R. F. Goodrich, B. A. Harrison, E. F. Knott and V. H. Weston

June 1966

Prepared for

Ballistic Systems Division  
Deputy for Ballistic Missile Re-entry Systems  
Air Force Systems Command  
Norton AFB, California

In addition to security requirements which apply to this document and must be met, this document is subject to special export controls and each transmittal to foreign governments or foreign nationals may be made only with prior approval of BSD (BSYDF), Norton AFB, Calif., 92409.

**SECRET**

# SECRET

7741-2-Q

## FOREWORD

This report was prepared by the Radiation Laboratory of the Department of Electrical Engineering of The University of Michigan under the direction of Dr. Raymond F. Goodrich, Principal Investigator and Burton A. Harrison, Contract Manager. The work was performed under Contract AF04(694)-834 "Investigation of Re-entry Vehicle Surface Fields (SURF)". The work was administered under the direction of the Air Force Ballistic Systems Division, Norton Air Force Base, California 92409 by Major A. Aharonian BSYDF and was monitored by Mr. Henry J. Katzman of the Aerospace Corporation.

The studies presented herein cover the period 18 March through 18 June 1966.

This report has been reviewed by BSD/Aerospace. The publication of this report does not constitute Air Force approval of the report's findings or conclusions. It is published only for the exchange and stimulation of ideas.

BSD Approving Authority

William C. Zeun  
Contracting Officer

# SECRET

**SECRET**

7741-2-Q

ABSTRACT

**(Secret)**

This is the Second Quarterly Report on Contract No. AF 04(694)-834 and covers the period 18 March to 18 June 1966. Progress on the SURF program is discussed. This program has as its objective the determination of the radar cross section of cone-sphere shaped re-entry vehicles by means of a study of the fields induced on the surface of vehicle models by incident radar energy. During this reporting period, some experimental difficulties involving the design of probes to measure tangential electric fields were resolved. Measurements were made of the electromagnetic properties of coating materials to be used in the study. Work on the theoretical basis for the prediction of the radar cross sections continued. Computations involving the re-entry environment are discussed.

**SECRET**

## TABLE OF CONTENTS

	Page
<b>ABSTRACT</b>	ii
<b>INTRODUCTION</b>	1
<b>Task 2.0 Experimental Investigations</b>	2
Task 2.1.1 Continuation of Measurements and Extension to Coated Bodies	2
Task 2.1.2 Frequency Variation	2
Task 2.1.3 Body Parameter Effects	2
Task 2.1.4 Effect of Discontinuities	7
Task 2.1.5 Shadow Boundary Effects	7
Task 2.1.6 Study of Coating Materials	7
Task 2.1.7 Far Field Measurements	12
Task 2.1.8 Antenna and Rocket Nozzle Perturbations	13
Task 2.1.9 Probe Design	13
Task 2.1.10 Concave Surfaces	22
Task 2.1.11 Absorber Fairings	22
Task 2.1.12 Plasma Sheath Experiments	22
Task 2.1.13 Design and Construction of Models	22
<b>Task 3.0 Theoretical Investigations</b>	26
Task 3.1.1 Analysis of Data and Computer Programming	26
A. Computer Program for Surface Currents and Radar Cross Section of Rotationally Symmetric Metallic Bodies	26
B. Comparison of Experimental and Theoretical Radar Cross Section Data for Metallic Cone-Sphere	40
Task 3.1.2 Effect of Surface Perturbations	43
Task 3.1.3 Spheroidal Surfaces	43
Task 3.1.4 Creeping Wave Theory	45
Task 3.1.5 Extension of Paraboloidal Solution to Paraboloidal Surfaces	48
Task 3.1.6 Effects of Coating Materials	48
Task 3.1.7 Radar Cross Section of the Cone-Sphere in a Re-entry Environment	48
<b>REFERENCES</b>	69

INTRODUCTION

This is the second Quarterly Report on Contract AF04(694)-834, "Investigation of Re-entry Vehicle Surface Fields (SURF)". It covers the period from 18 March to 18 June 1966. The objective of the SURF program is the determination of the radar backscattering properties of re-entry vehicles with shapes generally similar to the cone-sphere. The SURF program is monitored by Major Aharon A. Aharonian for the Ballistic Systems Division and Mr. Henry J. Katzman for the Aerospace Corporation.

The approach adopted in the investigation makes use of experimental measurements of the surface fields induced on various scale models of re-entry bodies and related shapes to aid in the construction of a theory to explain radar scattering behavior and in the formulation of mathematical expressions for the computation of radar cross section. In addition to the surface field measurements, backscatter measurements are relied on to furnish substantiation of the theory being developed or to guide the investigation in areas where surface field measurements alone do not provide adequate data. A digital computer program is being developed to study cases of oblique incidence on the target and cases where the radar backscatter is difficult to measure accurately.

The basic metallic cone-sphere with tip and termination modifications was studied during the first year of the SURF program. The results are summarized in the Final Report (7030-5-T) under Contract No. AF04(694)-683. The report is entitled "Radar Cross Section of the Metallic Cone-Sphere". In this year, it is planned to complete the work on the 'clean' cone-sphere and study the effect of absorber coatings, rocket nozzles and flush-mounted antennas on the radar cross section.

The continuing experimental investigation is described **under** Task 2.0 in this report and the experimental work is described under Task 3.0. The description, at this stage, is of the work in progress rather than of completed studies.

## TASK 2.0

### EXPERIMENTAL INVESTIGATIONS

#### Task 2.1.1 Continuation of Measurements and Extension to Coated Bodies

This is a "catch-all" task with goals duplicated or covered partially in other tasks. Viewed as a whole, it is approximately on schedule, or about 40 per cent complete.

The experimental study of cone angle variation upon surface fields has been performed for a cone-sphere coated with lossless dielectric material. Three cone angles were examined with  $ka=1.6$ , and a fourth angle was measured with  $ka=3.0$ . The measurements have been restricted to sharply tipped cone spheres and it is anticipated that only limited, if any, work will be done with coated, bluntly tipped models. The effects of protuberances on a bare object have only recently been started and will be mentioned under task 2.1.8.

Further work will include surface field measurements upon a coated cone-sphere for which the coating has magnetic as well as dielectric losses.

#### Task 2.1.2 Frequency Variation

This task is concerned with the electrical size of objects and with variations of the angle of incidence. During this reporting period several values of  $ka$  have been used, ranging from  $ka=1.0$  to  $ka=8.0$ , and only coated models have been measured, with attention restricted to nose-on incidence. It is expected that angle of incidence will not be studied until later. Task 2.1.2 is about 50 per cent complete.

#### Task 2.1.3 Body Parameter Effects

The effect of the travelling wave on the side of the cone is, of course, implied under Task 2.1.1 and we have already discussed variation of cone-angle there. Likewise, the effect of a blunted nose (radius= $b$ ) was discussed; it is observed in passing that the ratio  $b/a$  was to include the value unity, implying that a cylindrical model with hemispherical caps be examined. This shape has not been studied, nor indeed have we such a model, and unless required for the development of the theory, measurements will not be scheduled.

Task 2.1.3 also sets forth the thicknesses of the coatings to be examined, namely from 0.1 to 1.5 inches. The actual thicknesses employed in the laboratory will be determined largely by the materials themselves. We intend to use mostly commercial absorber sheets which are fortunately available in a variety of thicknesses ranging from 1/16 to 3/4 of an inch.

# SECRET

7741-2-Q

The travelling and creeping waves cannot be measured separately but the relative amplitudes of each can be obtained by an analysis of the data. The analysis has not yet been made for the case of coated cone-spheres but typical results which illustrate the behavior of these waves are shown in Figs. 2-2 and 2-3. The data, which appear in Figs. 2-2 through 2-3, are measurements of a cone-sphere having both lossless and lossy coatings with electrical sizes  $ka=1.0, 1.6, \text{ and } 5.0^*$ .

The geometry used is illustrated in Fig. 2-1. The incident wave is polarized horizontally and propagates along the direction of the cone-sphere axis. Both electric and magnetic fields were measured, each along a different path. A magnetic probe was oriented to sense the vertical component of magnetic field and the path traversed lay along the side of the model (in the plane of polarization). An electric probe was oriented parallel to the electric field and the path lay at the top of the model (in the plane perpendicular to the polarization). The two measurements were not, of course, made simultaneously. The surface field intensities were recorded as a function of distance from the tip.

The results for a lossless 3/8-inch thick coating and small  $ka$  are shown in Fig. 2-2. We are not certain what material forms the coating. Lincoln Laboratory which furnished the model has indicated Lucite. It is almost certainly low loss. Both the magnetic and electric fields show strong oscillations with an interesting contrast: the mean electric field is always weaker than the incident field while the mean magnetic field is always greater. The variations in electric field reach a minimum amplitude just forward of the join and the oscillations in magnetic field are relatively constant. The mean magnetic field attains a value about 2 db above the physical optics prediction for a conducting surface, indicating that the coating may be entraining energy. This suggests an enhancement of the creeping wave which in turn implies a larger and more widely varying cross section with increasing frequency than might be observed for an uncoated cone-sphere. It appears that lossless coatings should be avoided, as judged from surface field data.

A lossy coating was the material used for the data of Fig. 2-3, but the amount of loss is not known. The material was a dielectric coating of LS-22 (Emerson and Cuming) and we estimate the intrinsic loss to be 4.2 db per inch, based upon an extrapolation of higher frequency transmission line data. The oscillations in both electric and magnetic surface fields have smaller amplitudes than in the lossless case but the magnetic field is again still higher, and electric field still lower, than the respective incident field intensities. Of particular interest is the fact that the mean magnetic surface field is now 6 db above the incident field, which is only 3 db less than for the lossless case. The coating has a modest effect and the object is electrically short enough to restrict absorption of the travelling wave.

---

\* The radius,  $a$ , of the metallic spherical base is used to express size. Hence, no matter how thick the coating is,  $ka$  remains the same for a given frequency and a given cone-sphere.





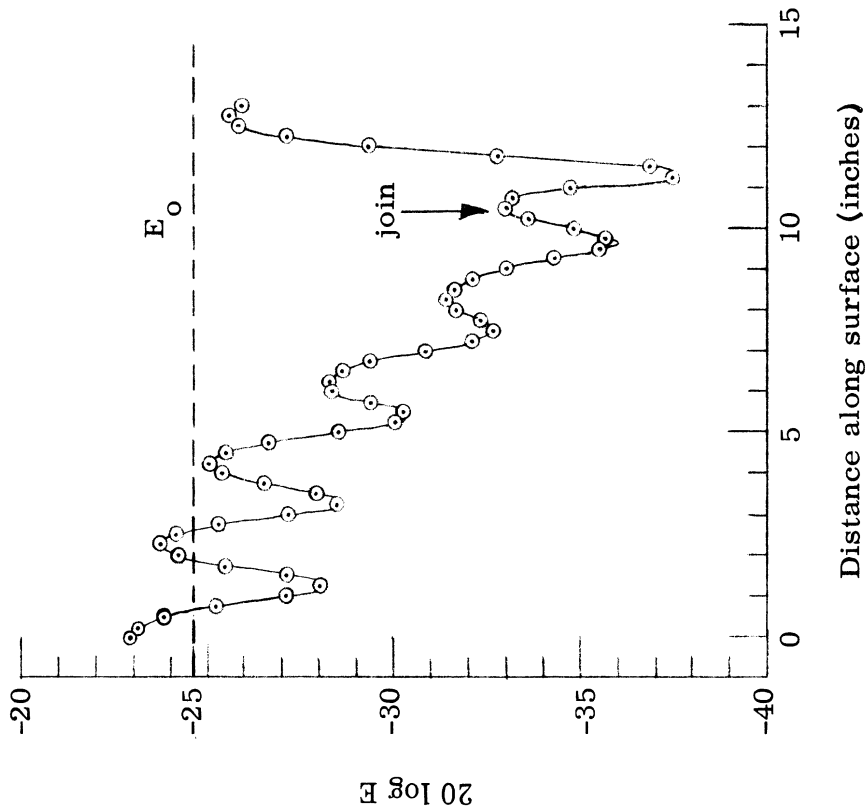
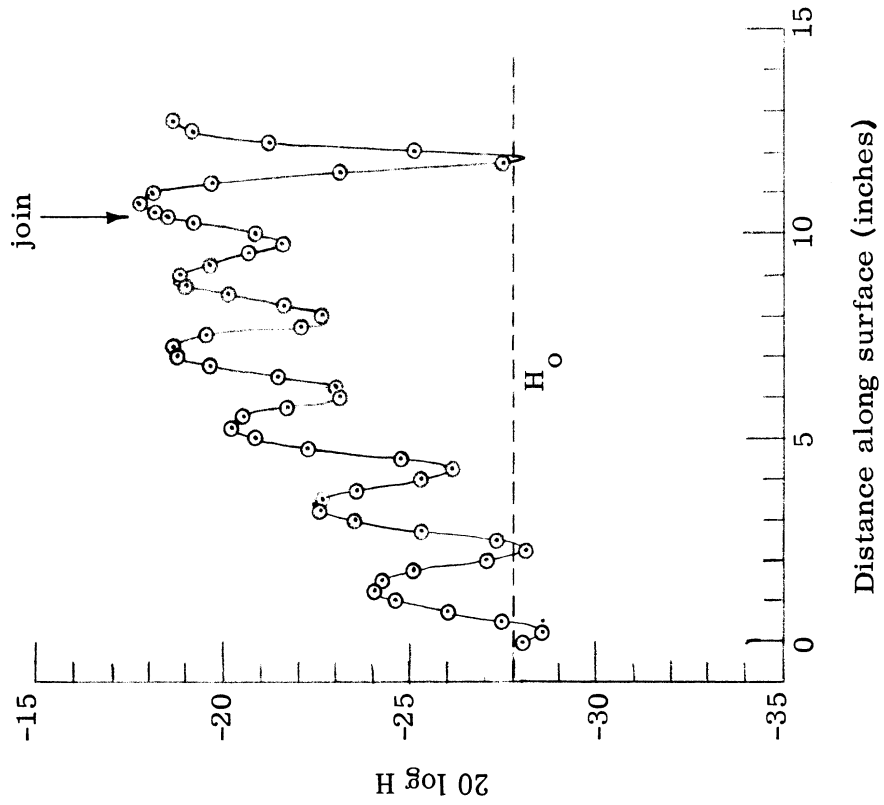


FIG. 2-2: SURFACE FIELD DATA FOR LUCITE-COATED CONE-SPHERE;  
 $ka = 1.6$ ,  $\alpha = 7.5^\circ$ ,  $\lambda = 3.97$  inches.

SECRET

7741-2-Q

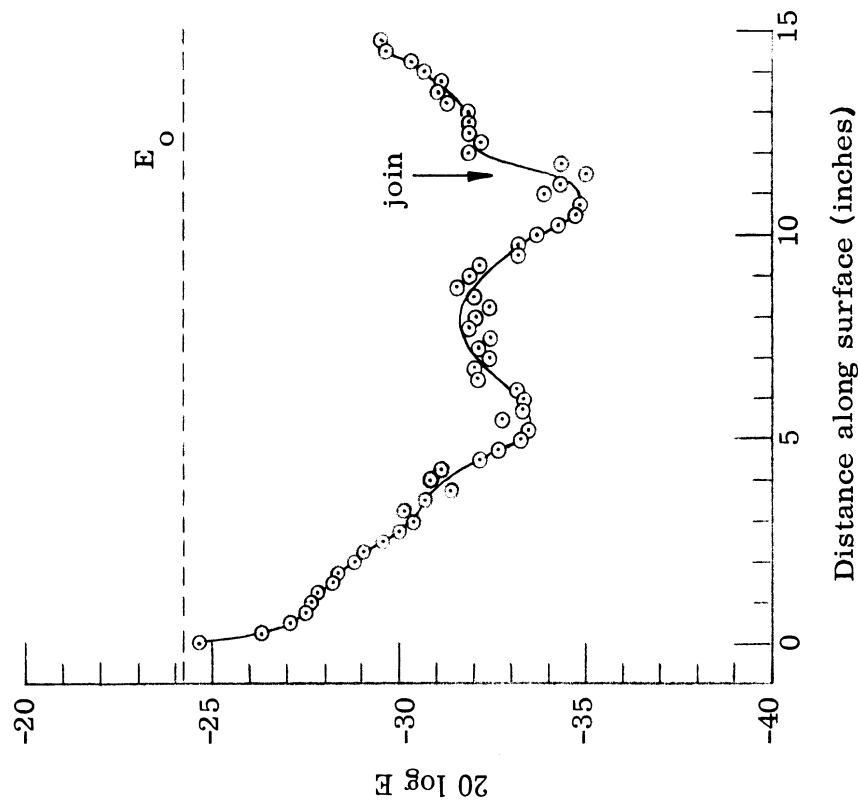
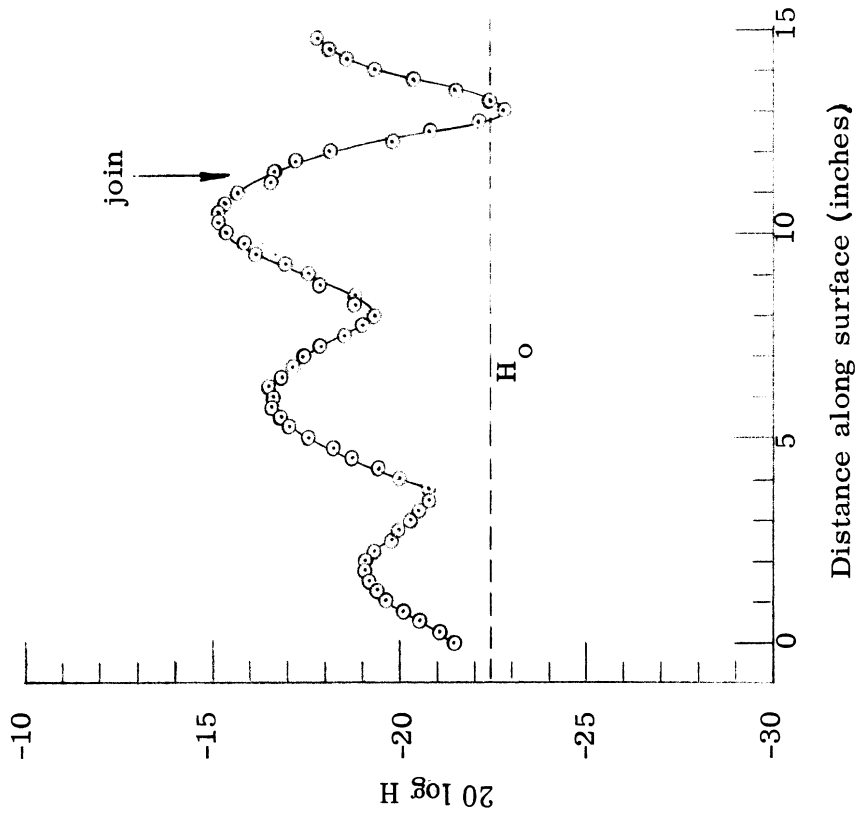


FIG. 2-3: SURFACE FIELD DATA FOR CONE-SPHERE COATED WITH LS-22 ;  
 $ka = 1.0$ ,  $\alpha = 7.5^\circ$ ,  $\lambda = 9.42$  inches.

9  
SECRET

Turning now to Fig. 2-4 we see the effect of a higher frequency, with  $ka=5.0$ . Although the same lossy coating was used, the material now has an estimated intrinsic loss of 20 db per inch. The electric field decays to approximately the same mean level as it did for  $ka=1.0$ , but there is a marked absence of oscillations (the reader is cautioned to observe the change of scale in passing from Figs. 2-2 and 2-3 to Fig. 2.4). The tiny wobbles that do appear have a period of  $\lambda$ , instead of  $\lambda/2$  as seen as lower values of  $ka$ , and we believe they are due to chamber reflections. This is not surprising in view of the high frequencies used and the small signal levels encountered. Note that the electric surface field falls off abruptly just beyond the join and that the magnetic field now also falls below the incident field level with widely swinging amplitude in the shadow region. The increased absorption of the material, coupled with the relatively long path length presented to the travelling wave, dramatically lowers the field intensity. The amplitude variations at the rear suggest the creeping wave is still present.

These data are typical of those being collected on coated objects. Coatings having magnetic losses have not yet been tested and may offer more challenge to measurement technique. On this basis the task is estimated to be 35 per cent complete.

#### Task 2.1.4 Effect of Discontinuities

This task encompasses the effects of discontinuities in surface curvature and derivative of surface curvature, and slight discontinuities in the penumbra, all for coated objects. No work per se has been performed, since the schedule calls for commencement of measurements at the beginning of the ninth month. In actual fact, however, this task could be considered under way, since an ordinary cone-sphere has a discontinuity in the curvature at the join and we have already examined coated cone spheres. The task is estimated to be 20 per cent complete.

#### Task 2.1.5 Shadow Boundary Effects

Effects of the confluence of the shadow boundary with surface discontinuities have not been measured but such a program is currently being started. Although this task was not intended to start until the beginning of the eighth month we expect measurements to begin before then. An indented-rear model is now available (Fig. 2-45) and measurements will be made after a current series of absorber measurements are complete. Depending upon the results, other terminations for this model may be necessary having varying degrees of curvature, and the model was designed to accept other base caps. Completion of this task is practically zero percent, since no data have been obtained.

#### Task 2.1.6 Study of Coating Materials

The goal of this task is to determine the absorbing quality of typical coatings by means of both surface field and backscatter measurements. We have chosen another route to accomplish this goal, namely by means of transmission line measurements.

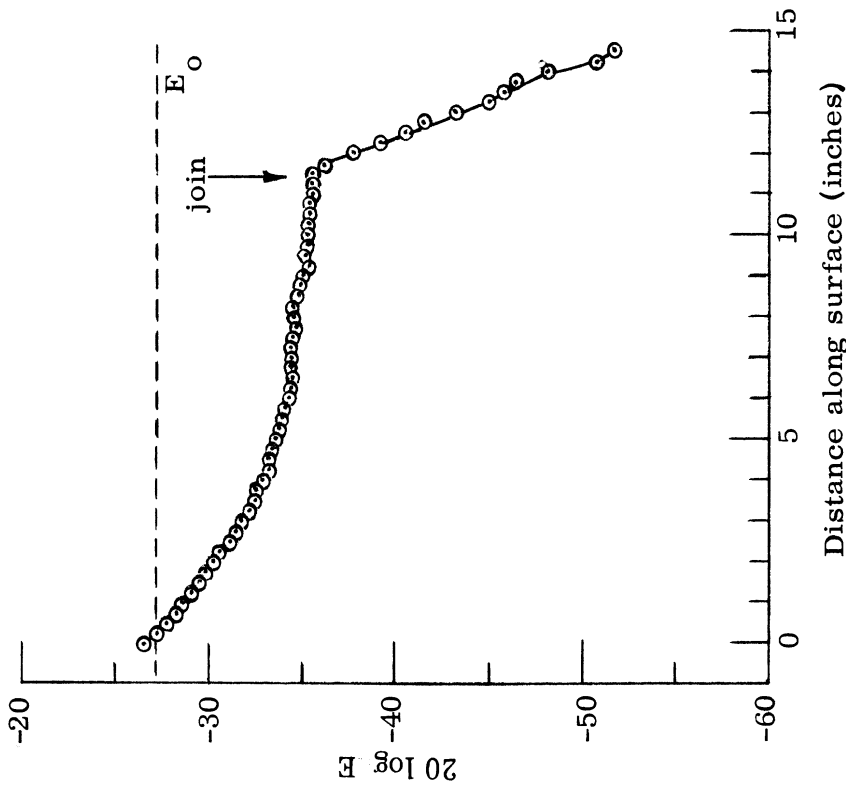
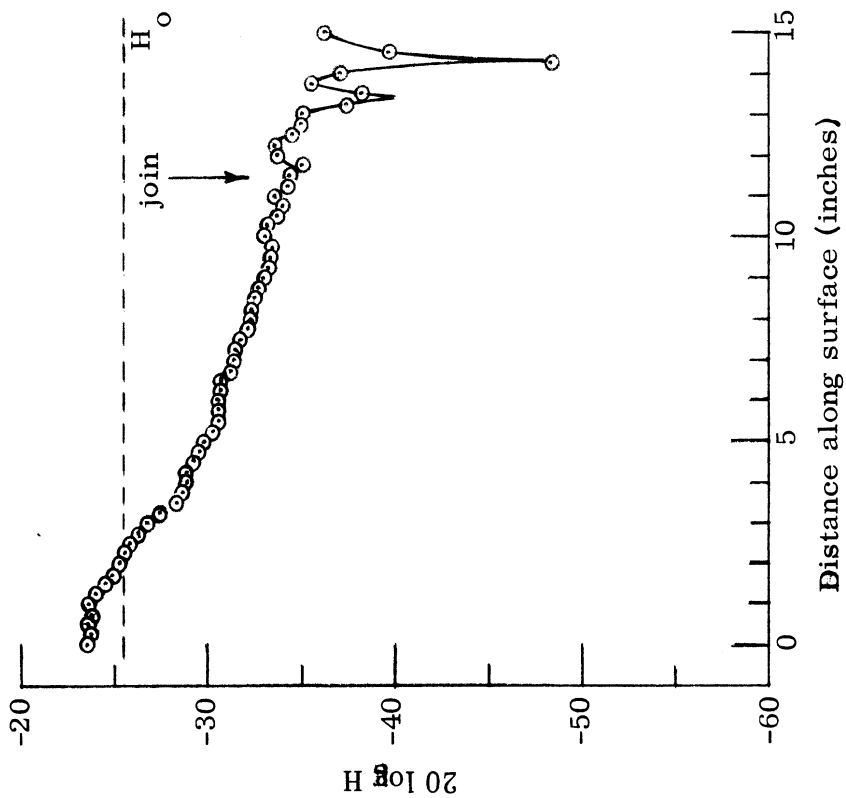


FIG. 2-4: SURFACE FIELD DATA FOR A CONE-SPHERE COATED WITH LS-22;  
 $ka = 5.0$ ,  $\alpha = 7.5^\circ$ ,  $\lambda = 1.88$  inches.

Slotted section techniques have been used to deduce the relative permittivity and permeability of several samples of readily available materials. These values, when the absorber thickness is known, permit us to evaluate absorber performance without the need for backscatter measurements.

The materials evaluation program, now being concluded, deals only with absorbers easily used under laboratory conditions and, in addition to those suited for the coating of models, others intended for uses such as waveguide terminations were measured. The latter will probably not be used directly in surface field studies, but will furnish a broader base for evaluation.

The measurements were hampered by equipment shortages and in some cases by difficulties in cutting the samples to the proper shape. The results show variations among otherwise identical samples which are possibly due to inhomogeneities in the parent materials; in spite of these and other sources of error, the results should be useful guides to the surface field and backscatter measurements in progress. A tentative list of results appears in Table I. Discussion of the measurements will appear in a subsequent Quarterly Report. Some discrepancies in the data are inherent in limitations of measurement techniques.

The transmission line technique yields much more information about an absorber than does ordinary backscatter measurements and the data are more versatile. The effect of thickness upon the power reflection coefficient, for example, can be quickly calculated from the complex  $\epsilon_r$  and  $\mu_r$ . Nonetheless, some coated flat plate backscatter work will be performed which will extend the frequency range of the transmission line measurements and which will give us a check of the values obtained thereby. Task 2.1.6 is estimated to be 90 per cent complete.

#### Task 2.1.6.1

Since the frequencies used in measurements to date have been in the L-, S- and C-band ranges, this task is 100 per cent complete.

#### Task 2.1.6.2

Measurements under this task include coatings upon flat plates, cylinder, and cone-sphere configurations, with emphasis on glancing incidence. No glancing incidence studies of cylinders and flat plates have been made. Such measurements will be difficult to interpret and contribute little to the understanding of the effects observed on coated cone-spheres. A few normal-incidence data have been obtained with cylinders and some normal incidence flat plate data will be acquired. The measurement of coated cone-spheres has been underway for several months and data have been obtained for four coatings, four cone angles and for four values of  $ka$ . Not all the possible combinations of the parameters have been examined since the inclusion of other variables rapidly advances the number of measurements to unrealizable proportions. Pending analysis of the data, some of the conditions not studied may be retroactively included if necessary. It is planned that three other coatings will be studied and the effects of incomplete coatings are reserved for Task 2.1.11. Task 2.1.6.2 is about 50 per cent complete.

#### Task 2.1.6.3.

The measurement of a 'typical' re-entry shape amounts to a modeling problem. In the full scale case, there may be a multilayered coating and possibly an oblate spheroid.

**MISSING  
PAGE**

**MISSING  
PAGE**



termination would be of interest. No measurements have yet been made of "typical" re-entry shapes.

### 2.1.7 Far Field Measurements

A few far field measurements have been made upon coated cone-spheres, and for the higher frequencies these have been difficult to obtain. The bare cone-sphere is already a low cross section shape and if even a mild absorber is added, the cross section attains values which tax our ingenuity to accurately obtain. These low cross sections present a series of problems and we have yet to satisfactorily solve them all. The measurements must take place in an anechoic chamber in which a CW system is used with a background **cancellation** scheme. When the coated object is installed upon a support column, its forward scatter disrupts the cancellation obtained in the absence of the target. Ordinarily such an effect can be evaluated and corrections can be made if the carriage bearing the column is moved in range, but since the nose-on backscatter is very small, the desired effect is **masked** by the column echo. Hence, the first problem to be solved is that of suppressing support column effects.

A useful way to avoid the overpowering effect of plastic foam columns is the use of string supports. The disadvantage of string suspension compared with a foam support is that the time required for a typical measurement greatly increases and that heavy models become difficult to handle. There is also a loss in aspect control due to inertia of the target, but this can be overcome at the expense of slower model rotation.

When the support problem has been solved we discover the nose-on cross section **can only be measured when the range is drastically reduced** to obtain acceptable signal-to-noise ratios in the receiving system. At these short ranges the incident power is not constant from tip to base, but decays by 1.5 db. In addition, when the target is viewed broadside the phase error (departure of the incident wave from being planar over the target length) can be of the order of 80 degrees, which is three times greater than that ordinarily acceptable.

As a compromise, measurements have been made at close range with a string support system to determine nose-on cross section and at a much greater range with a plastic foam column to determine the broadside through tail-on cross sections. Probably neither set of data gives the correct answer but, due to the limited schedule for backscatter work and this is the best that can be done for the present.

The backscatter program is incomplete but some interesting points can be made of the preliminary findings. It is possible, for example, to enhance the nose-on cross section of a cone sphere for small values of  $ka$  if one applies a poor coating. This may be due in part to the finite tip radius of a typical coating, (which is incidentally sutured on the target, since the coatings used so far have been flexible sheet foam) and/or because of the increased physical size. Also, tentative results suggest that cross section reduction far in excess of the absorber rating is possible, because of the relatively long absorbing path offered to the travelling wave at high frequencies.

# SECRET

7741-2-Q

We are still recording cross section patterns under this task, which is 50 per cent complete.

## Task 2.1.8 Antenna and Rocket Nozzle Perturbations.

This task is assigned to the study of perturbations of the bare cone-sphere and its commencement has been delayed in deference to work performed upon absorber-laden cone-spheres. Perturbations such as presented by external fixtures like rocket nozzles will be easy to simulate but the simulation of flush-mounted (slot) antennas is more difficult. This is because the impedance of a slot depends upon its depth and can be practically any value. We know from other studies that impedance loading is precisely the technique required for cross section reduction or modification and that quite different values can be obtained with relatively small physical adjustments.

A start has been made in which a small post is placed at one of several selected positions in the shadow. The post seems to have little effect on the creeping wave but apparently causes a reflection of energy that can enhance or suppress the creeping wave on one side. Data have been confined to measurements of surface current along the conical portion of the model just forward of the join. As might be expected, there are several places in the shadow at which the post has little effect. As work progresses, more posts or short cylinders will be used in an attempt to simulate rocket nozzles and positions with more precision.

Preliminary data will be collected for which slot antennas will be simulated by dipoles. A solitary dipole, probable a solid thin rod, will be used to verify that it is an independent scatterer and the measurements will eventually include several loaded dipoles. It should be pointed out that the impedances of these obstacles are in no way less frequency sensitive than those of slots; we seek to use them because of the ease with which they can be changed in the experimental program.

This task is 5 per cent complete.

## Task 2.1.9 Probe Design

In this task the capacity to measure phase is to be developed and the construction and use of electric probes is to be evaluated. The first part, that of measuring phase, has been completed and is described in Knott (1965). The phase system has been shown to work well. The second part, that of using electric probes, was beset with problems and was discussed in an earlier report. During this quarter the problems turned out to be less severe than was at first thought. Tangential electric fields can be measured near a conducting surface provided the probe is no closer than about  $\lambda/5$  and provided the radial electric field is not too strong. Evaluation of probe response suggests that under poor conditions a 2 db error is possible, but that in general the accuracy is better than this. The experimental procedure is described below. The test object used for the results summarized there was a sphere because of the exactness with which the fields may be predicted. A balanced magnetic probe is now

under construction and when completed should permit more accurate measurements to be made than were previously attainable. The probe is a back-to-back combination of the single unbalanced loop version used until now. The arrangement was chosen so that signals due to electric field sensitivity will arrive at the coaxial feed line out of phase and thus disappear from the total output signal. Development of the probe pictured in Fig. 2-5, is about 50 per cent complete.

#### Tangential Electrical Field Measurements Near a Sphere-Probe Evaluation

The purpose of the tests described here is to evaluate the probe designed to measure tangential electric field (Probe TD-H2) and assess existing capability for these measurements. At the surface of a perfect conductor there should be no tangential component of electric field, yet preliminary measurements indicated that the probe was sensing a finite field when it should not. The probe response to the supposed tangential field was very similar to that of the radial electric field.

Although too strong a signal was detected near the object, it was believed that Probe TD-H2 would sense the proper field if it were not too close to a conducting surface. In fact, in the absence of an obstacle, the far-field probe response was nearly a perfect cosine-squared pattern, which suggested that the probe was properly balanced and behaving normally.

Experimental Procedure . Figure 2-6 shows the probe and its accessories . The probe was made of two monopoles oriented  $180^\circ$  apart and positioned parallel to the incident wave. In order to use the probe, it must be balanced by summing the two signals from the monopoles. This is done by feeding the larger monopole signal through an attenuator, then to a hybrid tee while the other goes through a phase shifter to the hybrid tee. With the two probe leads connected this way, the phase shifter was adjusted for maximum output signal. The procedure was repeated to be sure of the settings.

The test object we used was a six-inch diameter aluminum sphere. A sphere was used because it is one of the few objects for which exact theoretical data can be obtained. The frequency used was 3.1308 Gc, which implies a  $ka$  of 5.00. Data were recorded in quarter-inch steps as the probe was withdrawn radially from the surface. Seven radial trajectories were used (Fig. 2-7) corresponding to azimuths between  $0^\circ$  and  $180^\circ$ , in  $30^\circ$  intervals. The quantity  $E_0$  is the field measured by the probe in the absence of the sphere and  $E$  is measured by the probe in the presence of the sphere. The ratio of  $E/E_0$  is plotted in Figs. 2-8 through 2-14 as a function of distance from the sphere surface.

Data. Theoretical data were obtained with the aid of a computer and were compared with the experimental results. Figures 2-8 through 2-14 show the comparison. The solid lines are the theoretical values and the datum points indicate the experimental values.

For all aspects, the theoretical and experimental values differ near the surface. At the surface, the theoretical values should be zero ( $-\infty$  db), but the experimental values are relatively high, ranging from -11 db to -28 db. We note that our equipment can sense a signal approximately 40 db below the incident field.



**SECRET**

7741-2-Q

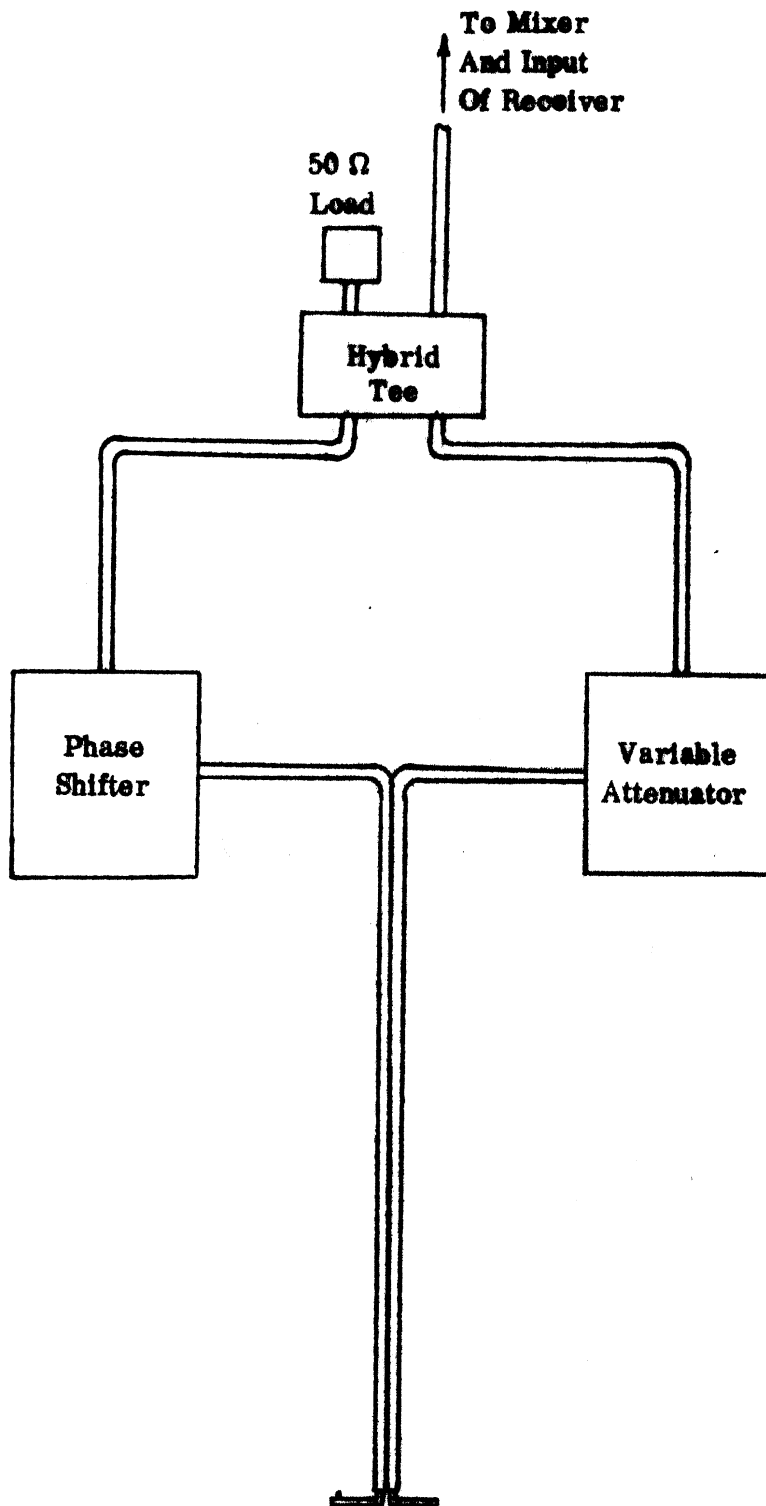


FIG. 2-6; ILLUSTRATION OF PROBE AND ACCESSORIES.

**SECRET**

SECRET

7741-2-Q

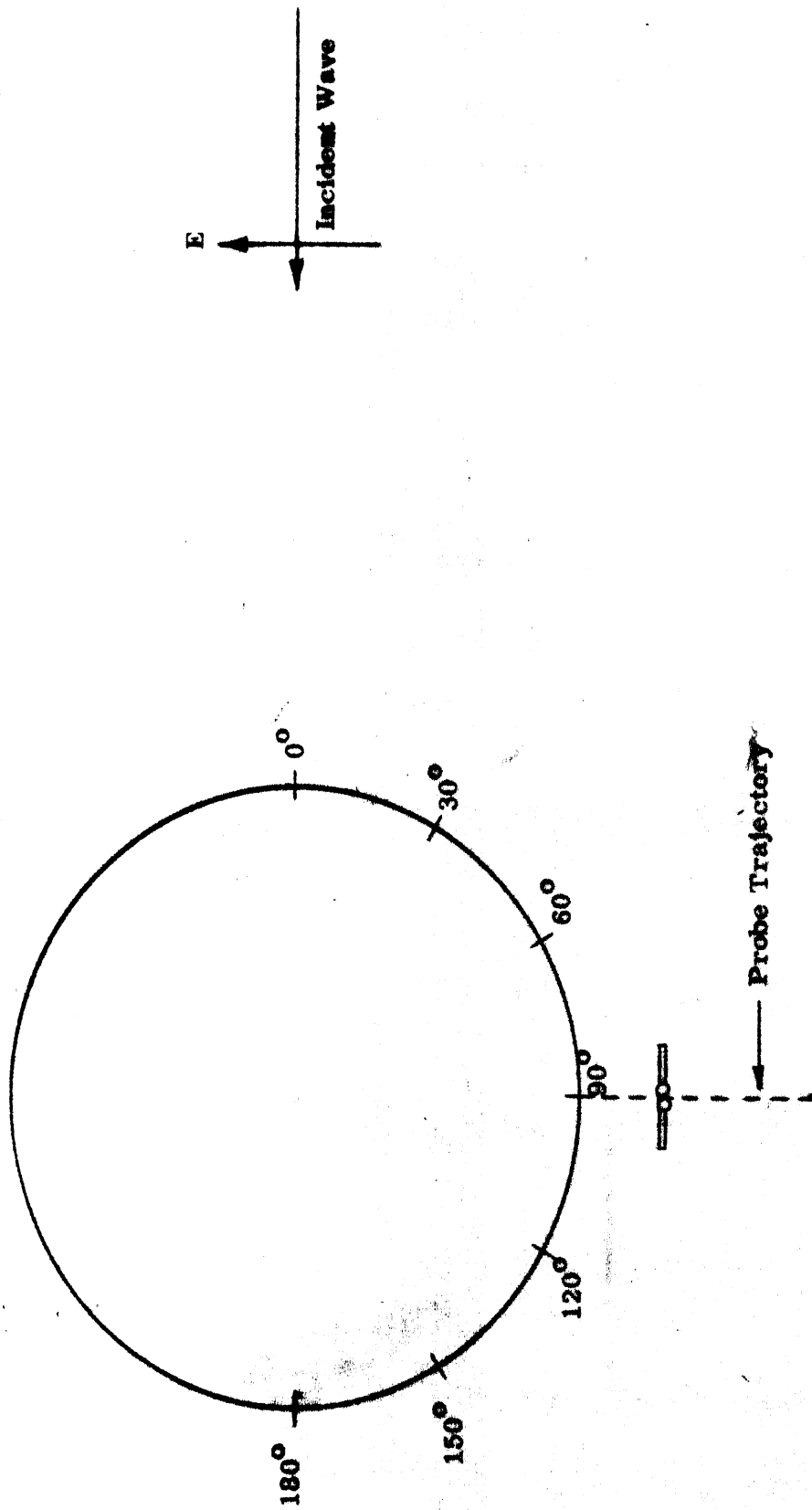


FIG. 2-7: TOP VIEW OF PROBE POSITIONING

SECRET

SECRET

7741-2-Q

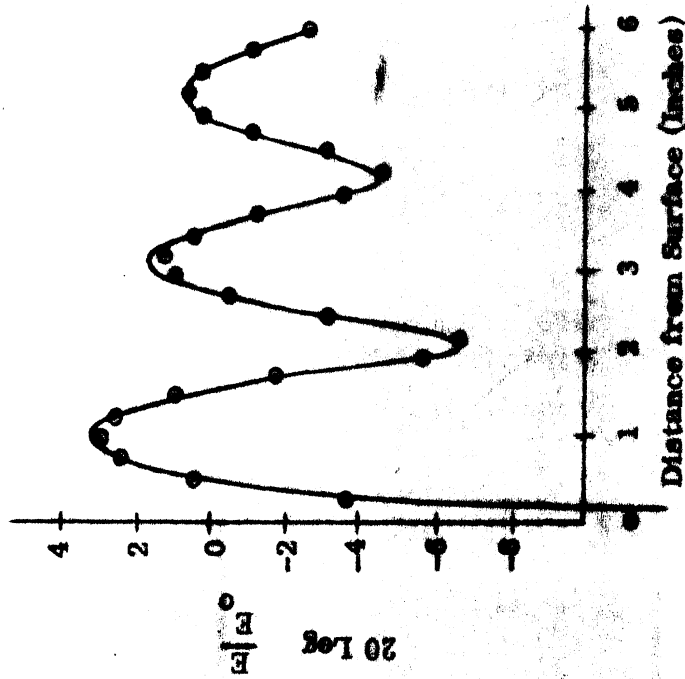


FIG. 2-9: AZIMUTH AT 30°

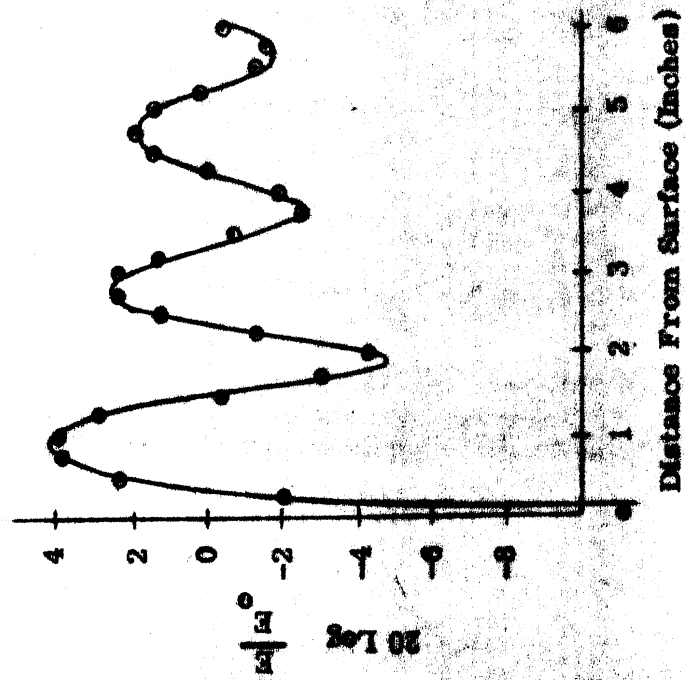


FIG. 2-8: AZIMUTH AT 0°

SECRET

SECRET

7741-2-Q

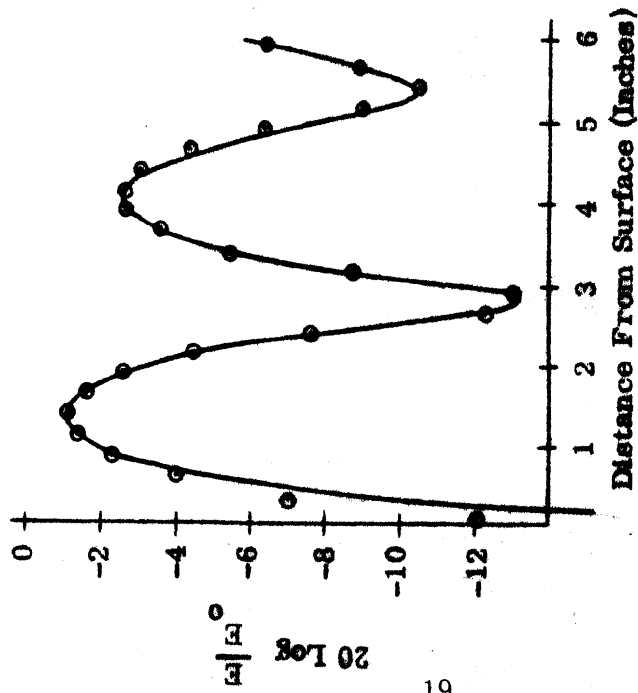


FIG. 2-10: AZIMUTH AT 60°

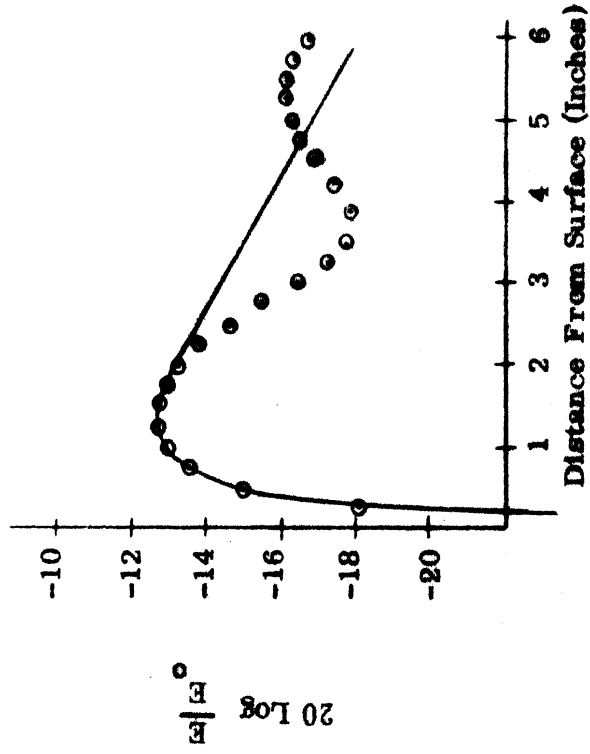


FIG. 2-11: AZIMUTH AT 90°

SECRET



SECRET

7741-2-Q

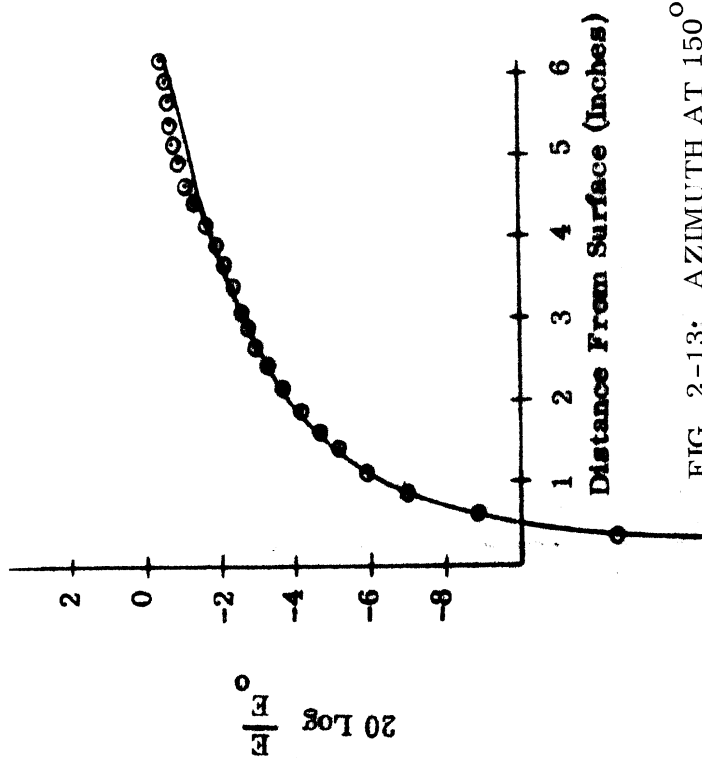


FIG. 2-13: AZIMUTH AT  $150^\circ$

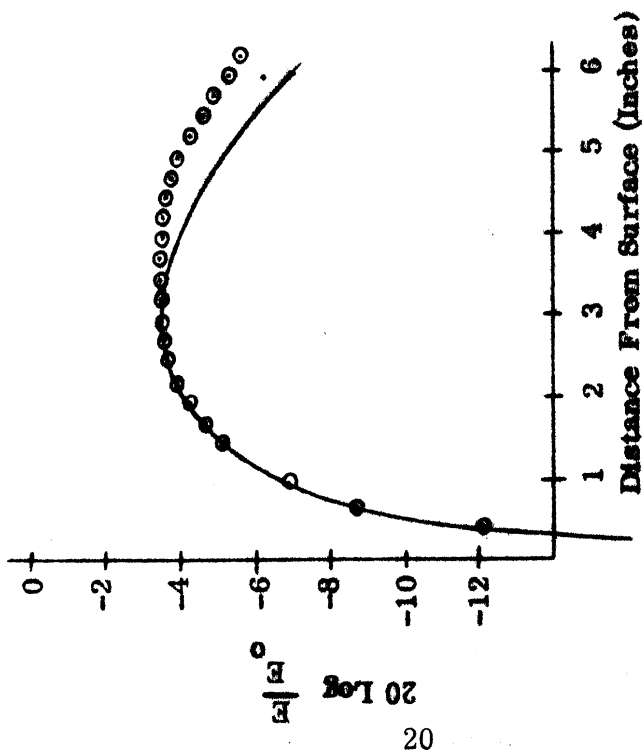


FIG. 2-12: AZIMUTH AT  $120^\circ$

SECRET

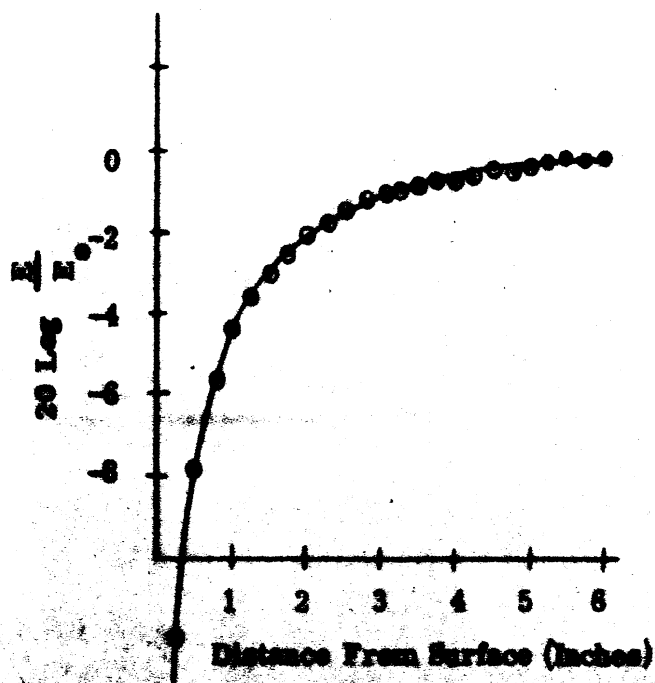


FIG 2-14: AZIMUTH AT 180°

Figures 2-8 through 2-10, 2-13 and 2-14 show a very good correspondence between theory and experiment for distances beyond about  $0.2\lambda$  from the surface. For the  $90^\circ$  aspect (Fig. 2-11), the correspondence is fair, but it should be noted that the field intensities are small. A slight misalignment of the probe might account for the difference between measured and computed values, but a more probable explanation is that the probe 'sees' an additional signal due to a strong radial electric field component. This is probably true for the  $120^\circ$  aspect also.

Conclusion. The agreement between experiment and theory is very good except near the surface of the sphere and for the  $90^\circ$  aspect. We believe the error for the  $90^\circ$  case is due to the sensitivity of the probe to the relatively intense radial electric field at that aspect. We think the data taken with this probe is accurate if the probe is held  $0.2\lambda$  from the surface and if the radial electric field is not too intense.

Task 2.1.10 Concave Surfaces

To study the effect of concavities in the rear of a re-entry body a model based upon the MK-12 has been constructed. The model has a separable rear portion which can be removed and replaced with ends of different degrees of concavity. The model is illustrated in Fig. 2-15. Measurements have not begun. They will be carried out concurrently with a theoretical study to determine how much experimental data is required to investigate the effect on the radar cross section due to deformations of the spherical part of the cone-sphere shape.

Task 2.1.11 Absorber Fairings

This task is concerned with studies of incomplete coatings, which may be of interest for weight savings or other reasons. The use of a partial coating may have merit and if so, is best used on the conical portion of the re-entry vehicle, but if the coating is abruptly terminated it may be a source of radar echo. The incomplete coating should be somehow faired into the conducting surface of the vehicle to remove the discontinuity and there are several ways to do this. In accord with the Program Plan the task has not yet been started.

Task 2.1.12 Plasma Sheath Experiments

This is the plasma task in which radar cross section will be measured under simulated re-entry conditions. The experiment will not be performed this year since the interesting and useful cases have not yet been selected. For those cases which appear useful, an oil bath arrangement or use of a ballistic range may be required for the proper simulation of plasma properties.

Task 2.1.13 Design and Construction of Models

Equipment and models are the subjects of this task, and during this quarter three models were constructed or are under construction.

A coated cone-sphere 3" in diameter and with a  $15^\circ$  angle (total) is still under construction. The object is to have a  $3/8$ " thick coating and samples of the material have been examined under the absorber evaluation program (Task 2.1.6). The coating has turned out to be very difficult to work with because it did not cure (it has a casting resin base) nor was it as machinable as stated by the manufacturer. We expect to coat future models with more familiar and more easily applied materials unless otherwise required. The coated model will not be measured until July.

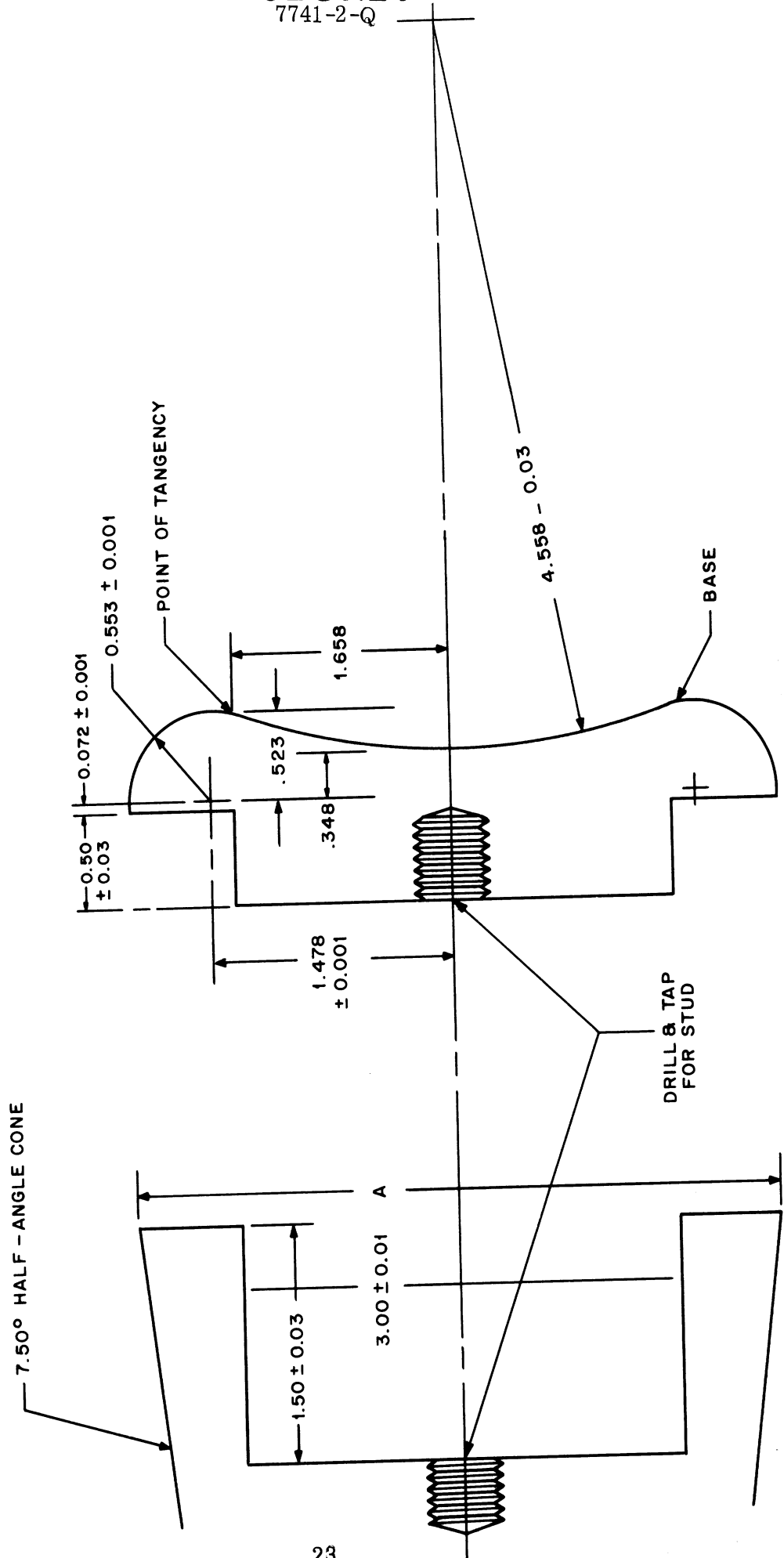


FIG: 2-15: MODEL FOR STUDY OF CONCAVE TERMINATIONS

An indented-rear model is now available for measurement. Depending upon the results, other terminations for this object having varying degrees of curvature may be constructed.

A model simulating a nose tip antenna is also under construction. This one uses the short conical portion and base of a cone-sphere previously used for blunted-nose experiments. The dimensions of the object are shown in Fig. 2-16. Both back-scatter and surface field measurements will be obtained and no doubt other dimensions and dielectric combinations will be suggested by the results.

A variety of models has been received from MIT and include some interesting shapes. Most of the models are cone-spheres, both bare and coated with low loss materials. Several different coatings appear on one size of these cone-spheres which may be of interest. Some objects having flares and join discontinuities were also received.

7741-2-Q

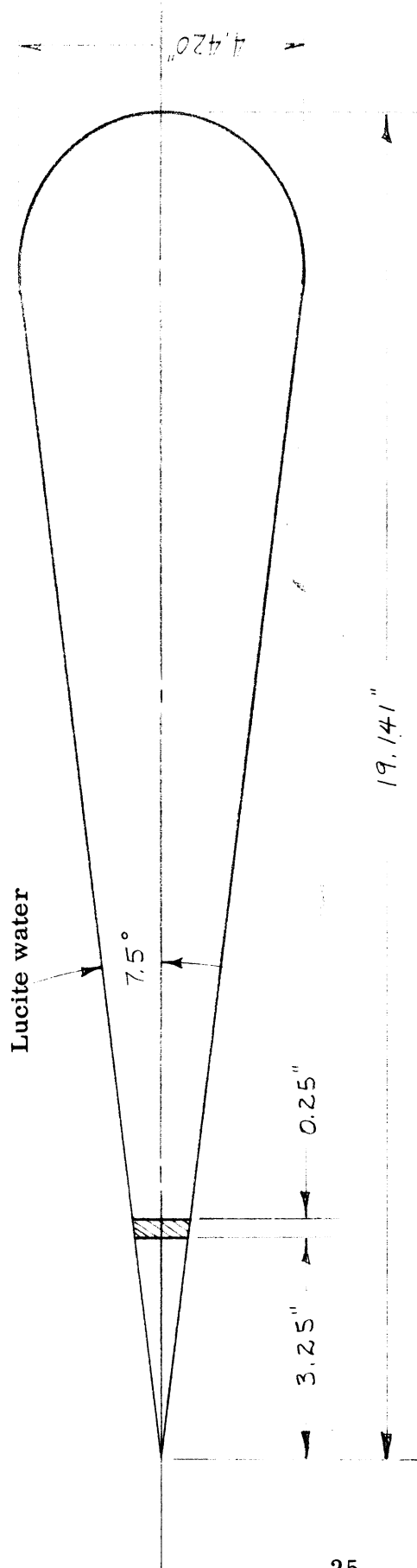


FIG. 2-16: NOSE-TIP ANTENNA MODEL

## TASK 3.0

## THEORETICAL INVESTIGATIONS

Task 3.1.1 Analysis of Data and Computer Programming

## A. Computer Program for Surface Currents and Radar Cross Section of Rotationally Symmetric Metallic Bodies.

1) Coated Shapes.

The analysis has been completed for computation of the surface fields for symmetric shapes satisfying an impedance boundary condition. This analysis will appear as a report. The programming will be essentially the same as for the perfectly conducting case. In fact, although the matrix appearing in this case is twice as large as that for the perfectly conducting case, it is reducible so that the inversion involves two inversions of matrices of the same size as in the perfectly conducting case. Physically, this is a result of there being no coupling between the polarizations. An analysis of the programming is given below. (Fig. 3-1).

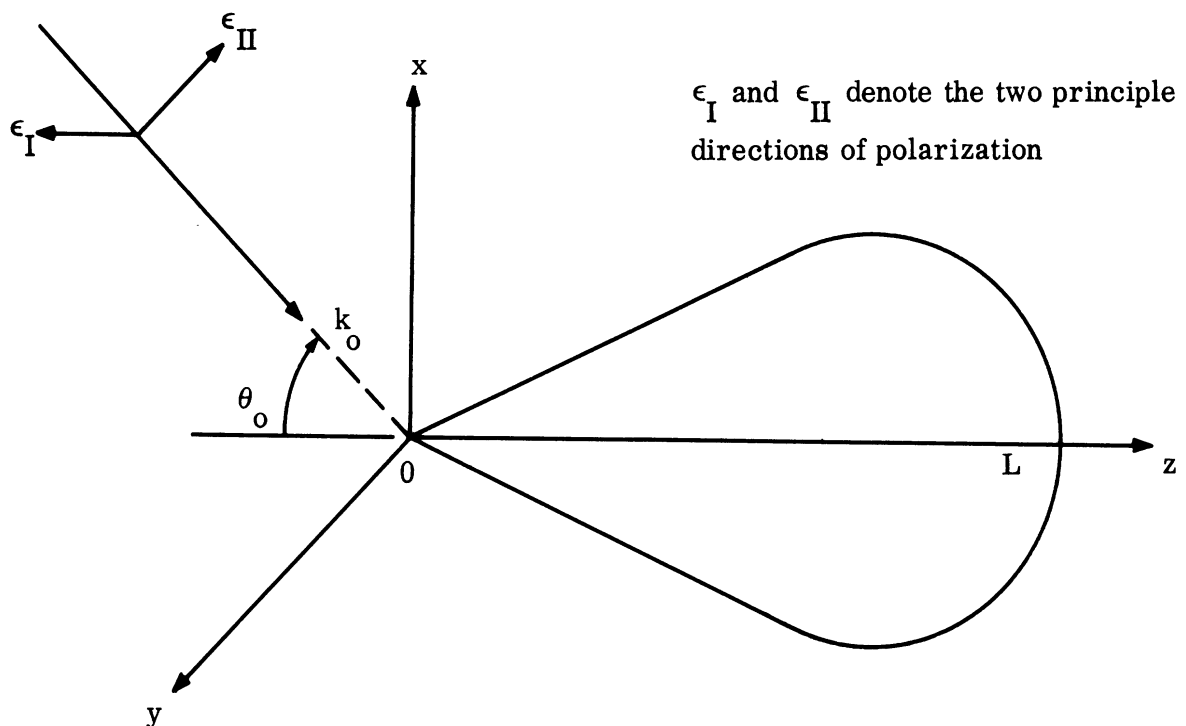


FIG. 3-1: COORDINATE SYSTEM FOR ROTATIONALLY SYMMETRIC PERFECT CONDUCTOR.

The incident electric field

$$\vec{E}^{(0)}(\vec{r}) = \vec{\epsilon} e^{j\vec{k}_0 \cdot \vec{r}}$$

is decomposed along the two principal directions

$$\vec{\epsilon} = a_I \hat{\epsilon}_I + a_{II} \hat{\epsilon}_{II}$$

and resolved into cylindrical modes, evaluated at the surface of the conductor

$$\begin{aligned} \vec{E}^{(0)}(\vec{r}) = & a_I \sum_{m=0}^{\infty} \left\{ E^{mI t}(z) \sin m\phi \hat{t} + E^{mI\phi}(z) \cos m\phi \hat{a} \right\} \\ & + a_{II} \sum_{m=0}^{\infty} \left\{ E^{mII t}(z) \cos m\phi \hat{t} + E^{mII\phi}(z) \sin m\phi \hat{a} \right\} + [\vec{E}^{(0)}(\vec{r}) \cdot \hat{n}] \hat{n} \end{aligned}$$

$\vec{r}$  on the surface.

If the incident electric field is, on the surface,

$$\vec{E}^{mI}(\vec{r}) = E^{mI t}(z) \sin m\phi \hat{t} + E^{mI\phi}(z) \cos m\phi \hat{a}$$

then the induced surface current is

$$\vec{K}^{mI}(\vec{r}) = K^{mI t}(z) \sin m\phi \hat{t} + K^{mI\phi}(z) \cos m\phi \hat{a} .$$

Similarly, if the incident electrical field is, on the surface

$$\vec{E}^{mII}(\vec{r}) = E^{mII t}(z) \cos m\phi \hat{t} + E^{mII\phi}(z) \sin m\phi \hat{a}$$



then the induced surface current is

$$\bar{K}^{mII}(\bar{r}) = K^{mIII}(z) \cos m\phi \hat{t} + K^{mII\phi}(z) \sin m\phi \hat{a} .$$

Now the true incident electric field is

$$\bar{E}^{(0)}(\bar{r}) = \sum_{m=0}^{\infty} \left\{ a_I \bar{E}^{mI}(\bar{r}) + a_{II} \bar{E}^{mII}(\bar{r}) \right\} + [\bar{E}^{(0)} \cdot \hat{n}] \hat{n} .$$

By superposition, the true induced surface current is

$$\bar{K}(\bar{r}) = \sum_{m=0}^{\infty} \left\{ a_I \bar{K}^{mI}(\bar{r}) + a_{II} \bar{K}^{mII}(\bar{r}) \right\} .$$

Consequently, one can solve for one mode-polarization at a time, and then use the expression above to get the total current.

This is the key-point in TRG's analysis.

The Boundary-Value Problem. We are faced with the problem: given an incident electric field which is, on the surface of the conductor,  $\bar{E}^{mI}$  or  $\bar{E}^{mII}$ , determine the induced surface current  $\bar{K}^{mI}$  or  $\bar{K}^{mII}$ .

The scattered field  $\bar{E}^{(s)}$  due to  $\bar{K}$  is given by

$$\bar{E}^{(s)}(\bar{r}) = \int ds' \bar{\mathcal{G}}(\bar{r}, \bar{r}') \cdot \bar{K}(\bar{r}')$$

where  $\bar{\mathcal{G}}$  denotes the Green's dyadic. The boundary condition for a perfect conductor is

$$\left[ \bar{E}^{(0)}(\bar{r}) + \bar{E}^{(s)}(\bar{r}) \right]_{\text{tor}\phi} = 0, \quad \bar{r} \text{ on } s .$$

The unknown induced current is expanded in terms of the complete set

$$\bar{K}(\bar{r}) = \sum_{n=1}^{\infty} C_n \bar{K}_n(\bar{r}), \quad \bar{r} \text{ on } s.$$

The induced electric field is

$$\bar{E}^{(s)}(\bar{r}) = \sum_{n=1}^{\infty} C_n \int ds' \nabla'(\bar{r}, \bar{r}') \cdot \bar{K}_n(\bar{r}').$$

Using this result in the boundary condition, dotting both sides with  $\bar{K}_m$  and integrating over the surface of the conductor, we obtain

$$\sum_{n=1}^{\infty} T_{mn} C_n = -b_m, \quad m = 1, 2, \dots$$

$$T_{mn} = \int ds \bar{K}_m(\bar{r}) \cdot \int ds' \nabla'(\bar{r}, \bar{r}') \cdot \bar{K}_n(\bar{r}'),$$

$$b_m = \int ds \bar{K}_m(\bar{r}) \cdot \bar{E}^{(0)}(\bar{r}).$$

In practice, we approximate  $\bar{K}$  by a finite sum

$$\bar{K}(\bar{r}) = \sum_{n=1}^N C_n \bar{K}_n(\bar{r})$$

and solve the  $N \times N$  set of truncated equations

$$\sum_{n=1}^N T_{mn} C_n = -b_m \quad m = 1, 2, \dots, N.$$

# SECRET

7741-2-Q

Choice of Trial Functions. For a particular mode-polarization, the unknown surface currents are given by

$$\bar{K}^m, I(\bar{r}) = K^{mIt}(z) \sin m\phi \hat{t} + K^{mI\phi}(z) \cos m\phi \hat{a}$$

or

$$\bar{K}^m, II(\bar{r}) = K^{mII t}(z) \cos m\phi \hat{t} + K^{mII\phi}(z) \sin m\phi \hat{a} .$$

We now have to guess the shapes of the unknown functions of  $z$ ,  $K^{m, I \text{ or } II, t \text{ or } \phi}$ .

It is convenient to consider the currents as functions of the normalized arc length  $t$  instead of the distance  $z$  along the axis of symmetry.

The trial shapes are

$$\bar{K}^{mI}(\bar{r}) = \sum_{n=1}^{N1} C_n^{mIt} K_n^{mIt}(t) \sin m\phi \hat{t} + \sum_{n=1}^{N2} C_n^{mI\phi} K_n^{mI\phi}(t) \cos m\phi \hat{a} ,$$

$$\bar{K}^{mII}(\bar{r}) = \sum_{n=1}^{N1} C_n^{mII t} K_n^{mII t}(t) \cos m\phi \hat{t} + \sum_{n=1}^{N2} C_n^{mII\phi} K_n^{mII\phi}(t) \sin m\phi \hat{a} .$$

For convenience in setting up the equations on the computer, we make the following simplifications:

- a) Set  $N1 = N2$ .
- b) We insist that the trial functions  $K_n^{m, I \text{ or } II, t \text{ or } \phi}$  be independent of the polarization (I or II), mode  $m$ , and the direction ( $t$  or  $\phi$ ).
- c) We required that the  $K_i(t)$ 's be dimensionless. The  $C$ 's will have the dimensions of current per unit length, per unit electric field.
- d) We want the  $K_i$ 's to be real. This simplifies the splitting of the quadratures for the  $b$ 's and  $T$ 's into real and imaginary parts.
- e) We shall renumber the ordering of the trial shapes so that the  $t$  and  $\phi$  directions are adjacent.

# SECRET

7741-2-Q

We assume for each mode  $m$  exactly  $N$  trial shapes

$$K_i(t) \quad i = 1, 2, \dots, N,$$

and construct a  $2N$ -parameter trial function

$$\bar{K}^{m, I}(\bar{r}) \approx \sum_{i=1}^N \left\{ C_{2i-1}^{mI} \sin m\phi \hat{t} + C_{2i}^{mI} \cos m\phi \hat{a} \right\} K_i(t),$$

$$\bar{K}^{m, II}(\bar{r}) \approx \sum_{i=1}^N \left\{ C_{2i-1}^{mII} \cos m\phi \hat{t} + C_{2i}^{mII} \sin m\phi \hat{a} \right\} K_i(t) \quad .$$

f) We will also assume the  $K_i(t)$  to be independent of the angle of incidence  $\theta_0$ .

The  $T$  matrix will then be independent of the angle of incidence, and need be calculated only once while investigating several directions of incidence. Since the trial functions are independent of polarization, it is unnecessary to evaluate the  $T$  matrix for both polarizations. It turns out that for  $m \geq 1$

$$T_{ij}^{mI} = (-)^{i+j} T_{ij}^{mII}$$

$$\left[ T^{mI} \right]_{ij}^{-1} = (-)^{i+j} \left[ T^{mII} \right]_{ij}^{-1}$$

so that only  $T^{mII}$  need be calculated.

This result allows a great simplification in storage, since only the  $T$ 's for the II polarization need be put on tape to be later withdrawn and inverted.

Since  $T_{ij}^{0I}$  and  $T_{ij}^{0II}$  never have non-vanishing elements at the same  $i$  and  $j$ , we store on tape the matrix elements for  $T_{2i, 2j}^{0I}$  and  $T_{2i-1, 2j-1}^{0II}$ .

In this fashion, we can store on tape, for each  $m$ , a single matrix  $T^m$  from which both  $T^{mI}$  and  $T^{mII}$  may be recovered. For the actual shape of  $K_i(t)$  we pick localized trial functions so that the  $T$ -integrals, e.g.

$$T_{2i-1, 2j-1}^{mI} = \frac{j\omega\mu C^2 K_0}{2} [1 - \delta_{mo}] \int_0^1 dt \int_0^1 dt' f(z) f(z') \cdot$$

$$\cdot \left\{ K_i(t) K_j(t') \alpha(z) \alpha(z') \left[ G_m + f'(z) f'(z') \frac{G_{m-1} + G_{m+1}}{2} \right] - Y_i(t) Y_j(t') G_m \right\},$$

go, not over the entire unit square, but over a small subportion. A convenient choice of trial function is obtained by approximating the  $K^{mIII t}(t)$  and  $K^{mIII \phi}(t)$  by piecewise-linear functions of  $t$ . We break the unit interval into  $N$  points  $0=t_0 < t_1 < \dots < t_N=1$  and sample the current at these  $N$  points. We define

$$C_{2i-1}^{mIII} = K^{mIII t}(t_i) \quad i=1, 2, \dots, N.$$

$$C_{2i}^{mIII} = K^{mIII \phi}(t_i) \quad i=1, 2, \dots, N.$$

= sampled values of the current, and draw straight lines connecting these sampled values.

This choice of piecewise-linear trial current is equivalent to the statement

$$K^{mIII t}(t) \approx \sum_{i=1}^N C_{2i-1}^{mIII} K_i(t)$$

$$K^{mIII \phi}(t) \approx \sum_{i=1}^N C_{2i}^{mIII} K_i(t)$$

The functions  $K_i(t)$  look as shown in Figs. 3-2a, b. This choice of trial functions makes the integrals for the  $T$ 's run over a small portion of the unit square and are consequently much less time consuming than over the unit square. For most of them a one point quadrature is enough.

Integrals over diagonal cells involve special treatment due to the singularity in the Green's function  $G_m$ .

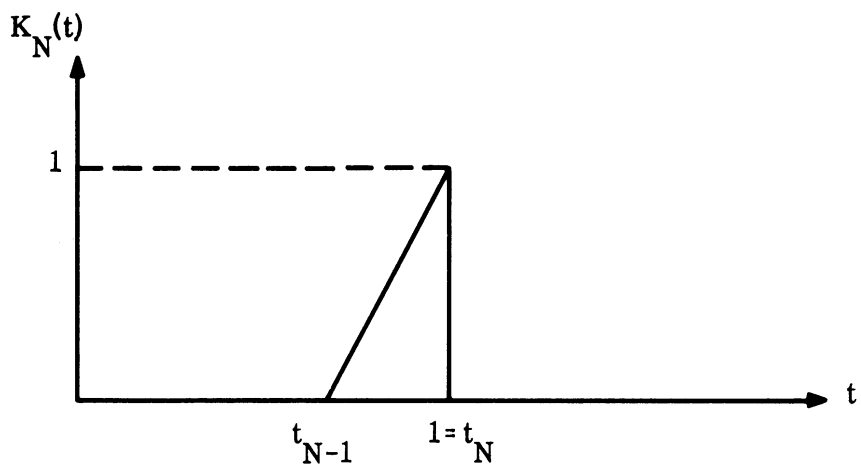
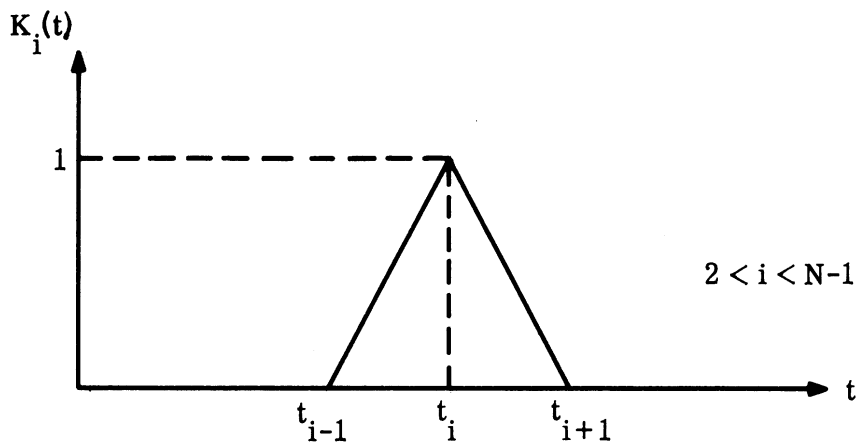
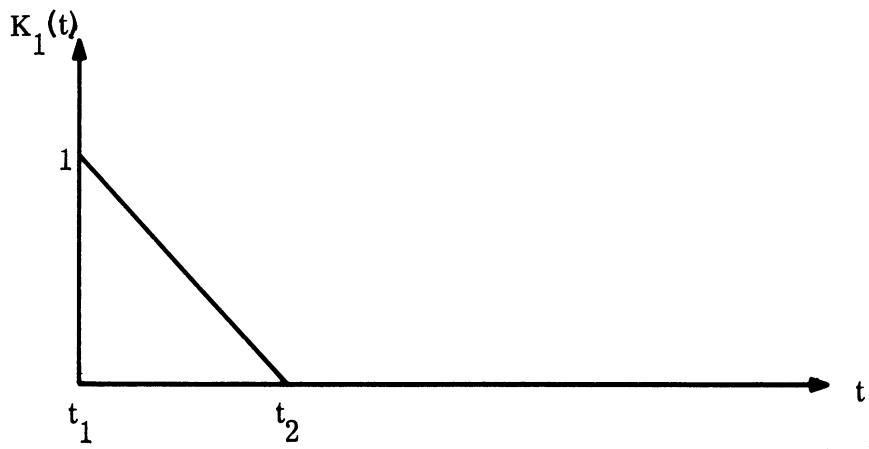
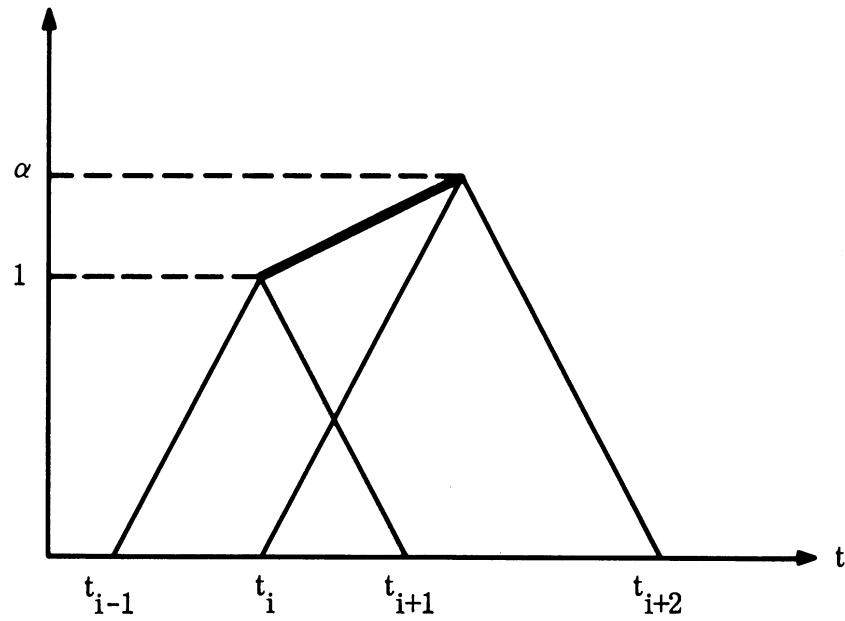


FIG. 3-2a: TRIAL SHAPES.



$$K_i^i(t) + \alpha K_{i+1}^i(t), \quad t_i < t < t_{i+1}$$

(**—**) Gives the segment.

FIG. 3-2b: TRIAL SHAPES.

The Green's function  $G_m$  is given by

$$G_m = \int_0^{\pi} d\theta \frac{e^{jk_o R} \cos m\theta}{k_o R}$$

The four adjacent matrix elements

$$T_{2i-1, 2j-1}^m \quad T_{2i-1, 2j}^m \quad T_{2i, 2j-1}^m \quad T_{2i, 2j}^m$$

go over the same (1 or 2 or most likely 4) cells, involving the same  $G_m$ , and, therefore, should be computed simultaneously.  $T^m$  for all  $m$  will be generated simultaneously, since it is efficient, for fixed  $z$  and  $z'$ , to generate all  $G_m(z, z')$ .

We use a scheme which uses the  $G$ 's immediately to compute the  $T$ 's, stores the  $T$ 's on tape and throws away the  $G$ 's. This is done in such a way that the  $G_m$ 's for a particular cell are used for all 16  $T$ 's which need them. The  $T$ 's must be stored on tape in a fashion which simplifies their inversion.

We use an inversion scheme which demands that the  $T$ 's be stored in a fashion that looks like the  $T$  matrix is being augmented by two rows and columns at a time.

That is, we want a storage procedure as shown in Fig. 3-3.

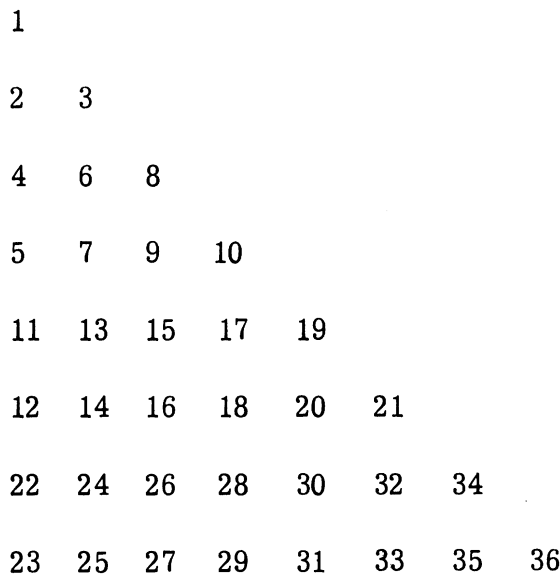


**FIG. 3-3: DESIRED STORAGE SEQUENCE  
AND PROPOSED SEQUENCE OF GENERATION.**



# SECRET

7741-2-Q

The elements labeled 1, 2, 3 can be generated simultaneously, as can elements 4-7, as can elements 8-10, as can elements 11-14, etc. Only a limited number of T matrix elements and G's are in core at one time. The  $G_m$ 's are stored for only one cell at a time. The  $G_m$ 's are stored for only one cell at a time. The generation scheme would be:

- a) Generate the  $G_m$ 's (all m) for cell C(1, 1).
- a') Compute T elements 1-3, and partially compute T elements 4-10.
- b) Generate the  $G_m$ 's (all m) for cell C(2, 1).
- b') Finish computing T elements 4-7, and partially compute T elements 8-15.
- c) Generate the  $G_m$ 's (all m) for cell C(2, 2).
- c') Finish computing T elements 8-10, and partially compute T elements 15-21.

The Inversion Scheme We recall that the  $T_{ij}$  are stored in a fashion which is equivalent to adding two rows and columns at a time. It is easy to verify that if

$$\begin{bmatrix} T^{(2p+2)} \end{bmatrix} = \begin{bmatrix} T^{2p} & E^{tr} \\ E & B \end{bmatrix}$$

then

$$\begin{bmatrix} T^{(2p+2)} \end{bmatrix}^{-1} = \begin{bmatrix} [T^{(2p)}]^{-1} & -F^{tr}WF & (-WF)^{tr} \\ -WF & W \end{bmatrix}$$

where

$$F = E [T^{(2p)}]^{-1} \quad 2 \times 2p \text{ matrix}$$

$$W = [B - FE^{tr}]^{-1} \quad 2 \times 2 \text{ matrix}$$

If the inverse of the upper  $2p \times 2p$  left-hand corner,  $T^{(2p)}$ , of  $T$  is known, then it is easy to compute the inverse of the upper  $(2p+2) \times (2p+2)$  left-hand corner  $T^{(2p+2)}$ . Since the  $T_{ij}$  are stored on tape in a fashion where two rows and columns are augmented at a time, this method of inversion is natural for the job. That is, we invert  $T^{(2)}$ , then  $T^{(4)}$ , then  $T^{(6)}$ , ..., and finally  $T^{(2N)}$ .

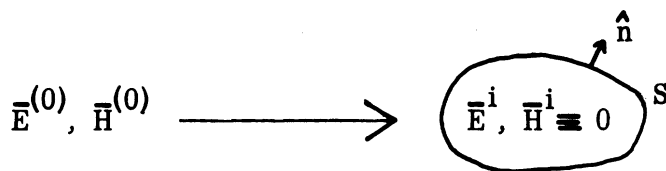
The storing of the  $T$ 's on tape is necessary in order to use an iterative refinement technique (Fig. 3-4) to improve the intermediate inverses.

With  $T^{-1}$  computed we obtain at once

$$C^{mIII} = [T^{mIII}]^{-1} b^{mIII}.$$

The entries of the column matrix  $C^{mIII}$  represent the sampled values of the current.

Extension to Coated Objects. The physical situation to be considered is



$$\bar{E}^{(0)}, \bar{H}^{(0)} \longrightarrow \left( \bar{E}^i, \bar{H}^i = 0 \right)_S$$

$$\begin{aligned} \bar{E} &= \bar{E}^s + \bar{E}^{(0)} \\ \bar{H} &= \bar{H}^s + \bar{H}^{(0)} \end{aligned}$$

with the boundary condition

$$(\hat{n} \times \bar{E}) \times \hat{n} = \eta Z \hat{n} \times \bar{H} \quad \text{on } S$$

that is,

$$\left[ \eta Z \bar{H} + \hat{n} \times \bar{E} \right]_{\tan} = 0 \quad \text{on } S.$$

The scattered fields are given by the well-known formulas

$$\bar{H}(\mathbf{s}) = \frac{1}{4\pi} \int_S \left[ i\omega\epsilon (\hat{n} \times \bar{E})\phi - (\hat{n} \times \bar{H}) \times \nabla\phi - (\hat{n} \cdot \bar{H}) \nabla\phi \right] ds,$$

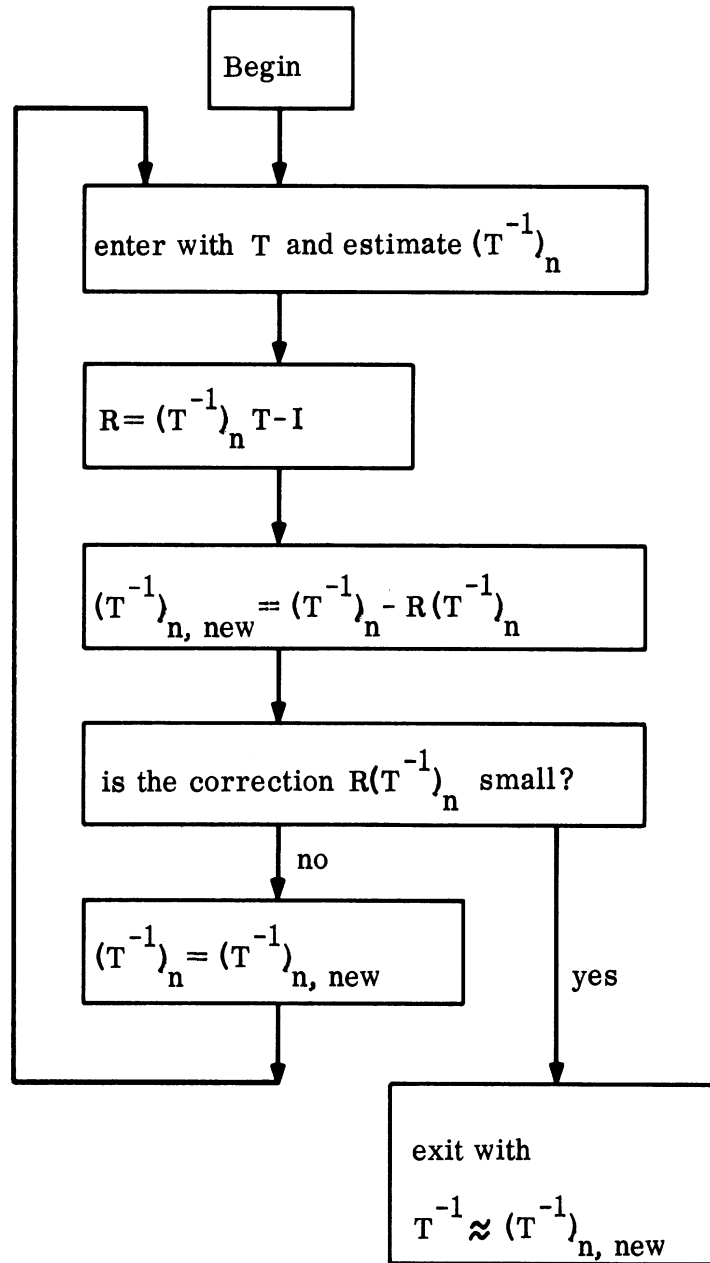


FIG. 3-4: ITERATIVE REFINEMENT LOOP.

$$\bar{\mathbf{E}}^S = -\frac{1}{4\pi} \int_S \left[ i\omega\mu (\hat{\mathbf{n}} \times \bar{\mathbf{H}}) \phi + (\hat{\mathbf{n}} \times \bar{\mathbf{E}}) \times \nabla\phi + (\hat{\mathbf{n}} \cdot \bar{\mathbf{E}}) \nabla\phi \right] ds .$$

The definitions

$$\begin{aligned} \bar{\mathbf{K}} &= -\hat{\mathbf{n}} \times \bar{\mathbf{H}}, & \bar{\mathbf{K}}^* &= \hat{\mathbf{n}} \times \bar{\mathbf{E}} \\ \sigma &= -\epsilon \hat{\mathbf{n}} \cdot \bar{\mathbf{E}}, & \sigma^* &= \mu \hat{\mathbf{n}} \cdot \bar{\mathbf{H}} \end{aligned}$$

together with the equations of continuity

$$\sigma^* = \frac{1}{i\omega} \left[ \text{div } \bar{\mathbf{K}}^* \right]$$

$$\sigma = \frac{1}{i\omega} \left[ \text{div } \bar{\mathbf{K}} \right]$$

plus the boundary condition

$$\hat{\mathbf{n}} \times \bar{\mathbf{K}}^* = \eta Z \bar{\mathbf{K}}$$

give for any exterior point

$$\bar{\mathbf{H}}^S = \frac{1}{4\pi} \int_S \left[ i\omega\epsilon \bar{\mathbf{K}}^* \phi + \frac{1}{\eta Z} (\hat{\mathbf{n}} \times \bar{\mathbf{K}}^*) \times \nabla\phi - \frac{1}{i\omega\mu} (\nabla \cdot \bar{\mathbf{K}}^*) \nabla\phi \right] ds$$

$$\bar{\mathbf{E}}^S = -\frac{1}{4\pi} \int_S \left[ -\frac{i\omega\mu}{\eta Z} \hat{\mathbf{n}} \times \bar{\mathbf{K}}^* \phi + \bar{\mathbf{K}}^* \times \nabla\phi - \frac{\bar{\mathbf{K}}^* \cdot (\nabla \times \hat{\mathbf{n}})}{i\omega\epsilon \eta Z} \nabla\phi + \frac{\hat{\mathbf{n}} \cdot (\nabla \times \bar{\mathbf{K}}^*)}{i\omega\epsilon \eta Z} \nabla\phi \right] ds .$$

If the field point is now allowed to approach the surface, proper account must be taken of the discontinuous behavior of the integrand after the manner of **Maue**.

This is accomplished by use of the results:

1) If  $\bar{\mathbf{A}}$  is a vector field tangent to  $S$ , and  $\bar{\mathbf{r}}_0$  is a point of  $S$ , then the integral

$$\bar{\mathbf{I}}(\bar{\mathbf{r}}) = \int_S \bar{\mathbf{A}}(\bar{\mathbf{r}}') \phi(\bar{\mathbf{r}}, \bar{\mathbf{r}}') ds'$$

is continuous for all  $\bar{r}$ .

$$2) \quad \hat{n}(\bar{r}_0) \times \lim_{\bar{r} \rightarrow \bar{r}_0} \int_S \bar{A}(\bar{r}') \times \nabla \phi \, ds' = \pm 2 \bar{n} \bar{A}(\bar{r}_0) + \int_S \hat{n}(\bar{r}_0) \times [\bar{A} \times \nabla' \phi] \, ds' \quad .$$

In the left-hand member, the approach  $\bar{r} \rightarrow \bar{r}_0$  is along the normal to  $S$ . In the right-hand side, the plus and minus signs correspond, respectively, to an approach from the outside and from the inside of  $S$ .

When these results are used in the former integral relations, and  $\bar{E}^s$  and  $\bar{H}^s$  are combined on the surface with the aid of the boundary condition

$$\left[ \eta Z (\bar{H}^s + \bar{H}^{(0)}) + \hat{n} \times (\bar{E}^s + \bar{E}^{(0)}) \right]_{\tan} = 0$$

one obtains one vector integral equation corresponding to two coupled Fredholm integral equations of the second kind.

The same form of analysis used for the perfectly conducting case can now be applied to these equations. The presence of the unknown outside the integral sign only affects the diagonal elements of the matrix.

## 2) Schweitzer Inversion.

The Schweitzer inversion using a bordering technique and including the refinement loop has been successfully programmed. The convergence is very rapid.

### B. Comparison of Experimental and Theoretical Radar Cross Section Data for Metallic Cone-Spheres.

In Figs. 3-5 and 3-6, a comparison is shown between radar cross section measurements and theoretical computed values for metallic cone-spheres. The experimental values were obtained by AVCO Corporation (1966) at their scattering range. The models they used were aluminum cone-spheres of different sizes and with  $16^\circ$  and  $30^\circ$  total cone angles. The  $16^\circ$  cone-sphere was a scaled model of the LORV re-entry vehicle except that the tip of the cone was not rounded. The measurements were made at frequencies between 33 and 36 Kmc which corresponded to  $ka$  values between 3.50 and 5.36 for the  $16^\circ$  models. This is equivalent to a frequency range for the full-size LORV L-8 re-entry vehicle of 318.8 to 480 Mc.

The theoretical values were computed from the Fortran II program which was given in the Appendix of the draft of the Final Report of the first year's SURF investigation (1965): The program, for the pointed tip cone-sphere, was used to compute numerical data for equations (4.16) and (4.17) of that report.

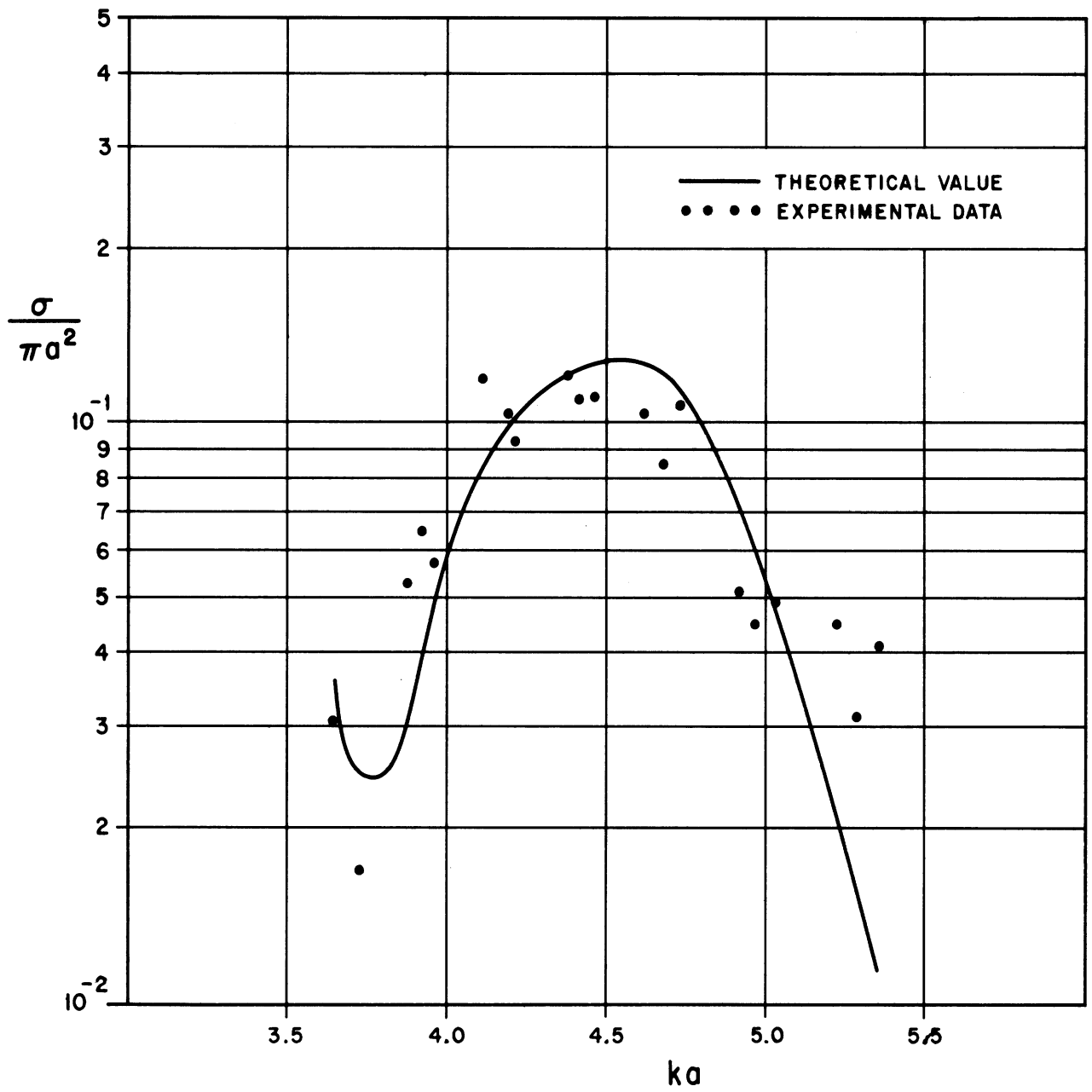


FIG. 3-5: COMPARISON OF EXPERIMENTAL AND THEORETICAL RADAR CROSS SECTION DATA FOR A 15° HALF-ANGLE METALLIC CONE-SPHERE.

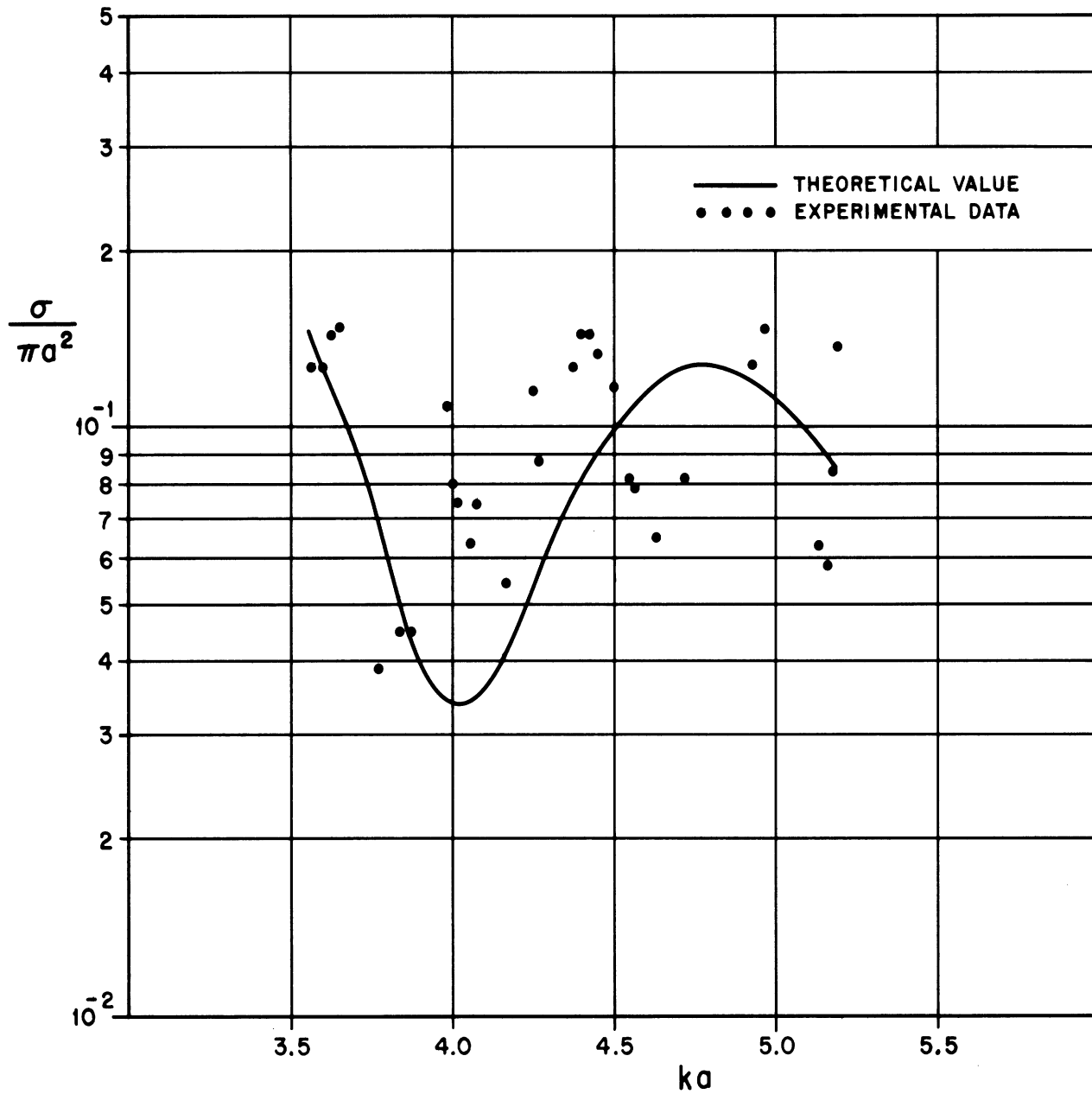


FIG. 3-6: COMPARISON OF EXPERIMENTAL AND THEORETICAL RADAR CROSS SECTION DATA FOR AN  $8^\circ$  HALF-ANGLE METALLIC CONE-SPHERE.

On examining the comparison shown in Fig. 3-5 for the 15° half-angle cone-sphere one finds that the experimental and theoretical values are in excellent agreement. The experimental points exhibit the slight randomness associated with experimental error but follow the computed curve with an average deviation of only 0.3 db.

The 8° data has an oscillation within the given ka range with an apparent period which is three times that which would be predicted from theoretical considerations. This oscillation is contrary not only to what has been indicated by theoretical computations for all half-cone angles studied but also to that shown by compilations of experimental data from all other sources. Both empirical and computed data show only a single period, such as that given by the solid line in Fig. 3-6, rather than the multiple period produced by the 8° data. It is possible that the method of mounting the model (e.g.) or some extraneous scatterer in the room in which the measurements were made was the source of an interference phenomenon. Nevertheless, the data, in spite of its dispersion, falls within the region of the computed curve. The average deviation is 4.5 db. Referring again to the 15° case, one can see that the theoretical curve can be relied upon to give extremely accurate results for the radar cross section of the metallic cone-sphere. The 8° theoretical curve which is not subject to experimental error and random interference, would have given a more reliable answer than that obtained from the experimental measurements.

### Task 3.1.2 Effect of Surface Perturbations

Consideration is being given to determine the best methods for modeling slot antennas by the use of dipoles or other simple structures attached to the surface of metallic cone-sphere models. Experiments are being designed to obtain data in the surface field measurement facility and in the backscatter range so that the equivalence of simple structures to slots may be demonstrated. This work has not reached a stage at which detailed analysis is ready for presentation.

### Task 3.1.3 Spheroidal Surfaces

We approach the problem of the scattering of an electromagnetic plane wave by a perfectly conducting spheroid from the observation that the incident and scattered field are reducible under the angular momentum operator. We have that the incident field has a representation

$$\vec{\psi}_o = \sum_{J, \ell, M} b_{J\ell}^M y_{J\ell}^{\vec{M}}$$

the scattered field a representation



# SECRET

7741-2-Q

$$\vec{\psi}_s = \sum_{J\ell M} c_{J\ell 1}^M \vec{Y}_{J\ell 1}^M$$

where the  $\vec{Y}_{J\ell 1}^M$  are vector spherical harmonics (Wigner, 1931). However, the field is not reducible in the neighborhood of the spheroid, within the sphere of minimum radius which bounds the spheroid. The conclusion from this observation is that there is coupling between the angular momentum components in the scattering process. If, now, we can determine the form and strength of this coupling we conjecture that we have uncovered the essential difference between the sphere problem in which there is no coupling and the non-sphere problems in which the coupling always obtains.

Our analysis starts with the representation of the spheroid solution by F. V. Schultz (1950) in terms of the scalar spheroidal wave functions. Briefly, the incident field is represented by

$$\vec{\psi}_o = \sum_n \nabla_x \vec{A}_n^o \psi_n^{o1}$$

where the  $\psi_n^{(1)}$  are the spheroidal wave functions

$$\psi_n^{(i)} = S_n^o(i)(\xi, \gamma) P_s_n^o(\eta, \gamma^2)$$

where we use the notation of Meixner and Schäfer (1954) for the spheroidal function. Taking a similar representation for the scattered field

$$\vec{\psi}_s^{-1} = \sum_n \nabla_x \vec{A}_n \psi_n^{(3)}$$

the application of the perfectly conducting boundary condition leads to a matrix equation for  $\vec{A}^{-1}$  in terms of  $\vec{A}_o$ , say,

$$\vec{A} = M^{-1} \vec{A}_o$$

We now make the observation that the spheroidal wave functions can be expanded in terms of the spherical wave functions

$$\psi_{\ell m}^{(j)}(F) = z_{\ell}^{(j)}(kr) P_{\ell}^m(\cos \theta) e^{im\phi}$$

where  $z_{\ell}^{(j)}$  is a solution of the "spherical" form of Bessel's equation. Symbolically,

$$\psi^{(j)} = T \psi_s^{(j)}$$

and

$$\psi_s^{(j)} = T^{-1} \psi^{(j)}$$

From the above we can represent the coupling between the incident and scattered angular momenta in terms of the matrix,

$$M = T M^{-1} T^{-1}$$

The difficulty in continuing the analysis lies in the inversion of the matrix M. For this reason we are at present considering two simplified cases

- 1) If the spheroid is very near a sphere then M is a diagonally dominant  $M^{-1}$  can be approximated.
- 2) If the frequency is low enough M can be truncated and the approximate inversion found directly

We are proceeding with these analyses having encountered no great difficulty but have not yet achieved any definitive results.

#### Task 3.1.4 Creeping Wave Theory

The integral equation approach to creeping waves on a general surface is being checked against the refined creeping wave representation of the surface fields on a sphere. On the comparison the two agree except for a factor of 2 in one term. This we believe is due to an algebraic error which we are confident of finding.

The outline of this work as presented at the Technical Discussion meeting is included below.

##### Theory of Creeping Waves

A theoretical method for obtaining the creeping wave contribution from a smooth convex body is outlined. After the theoretical solutions are obtained, the results will be applied to estimate the radar cross section of a cone with non-spherical termination (cone-spheroid, etc.) in the resonance region.

A. Scalar Problems.

$$U(\mathbf{F}) = 2 U_0(\mathbf{F}) - \frac{1}{2\pi} \iint da' U(\mathbf{F}') \frac{1 - ikR}{R^3} \left\{ \bar{\mathbf{N}}(\mathbf{F}') \cdot \bar{\mathbf{R}} \right\} e^{ikR}$$

where  $\bar{\mathbf{R}} = \mathbf{F}' - \mathbf{F}$

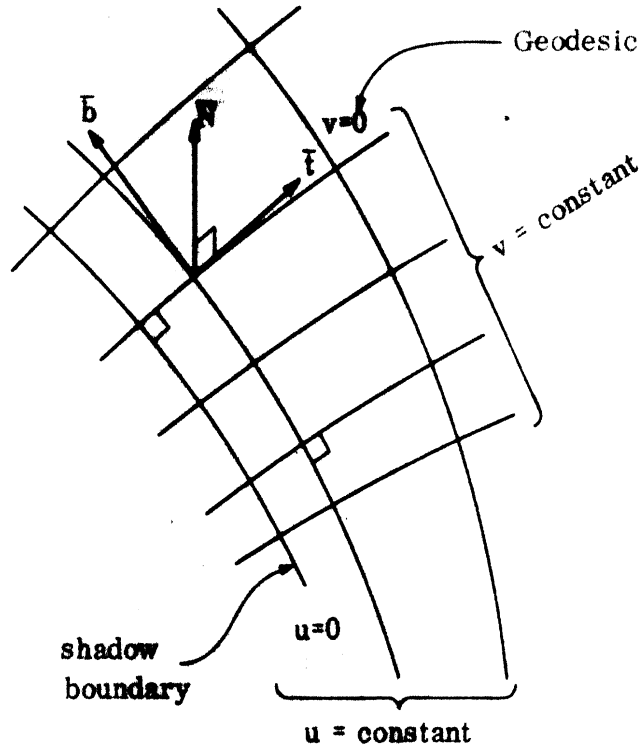


FIG. 3-7: GEOMETRY OF THE BOUNDARY

Basic Relationships for the Geodesic coordinate

$$dl^2 = du^2 + G(u, v) dv^2$$

$$da = \sqrt{G} dudv$$

The Gauss equations

$$\begin{cases} \frac{\partial \bar{t}}{\partial u} = -\kappa_g \bar{\mathbf{N}} \\ \frac{\partial \bar{t}}{\partial v} = \frac{\partial \bar{b}}{\partial u} = \kappa_{tt} \\ \frac{\partial \bar{b}}{\partial v} = -G \left\{ \kappa_{tt} \bar{\mathbf{t}} + \kappa_{tn} \bar{\mathbf{N}} \right\} \end{cases}, \quad (\kappa_t = \sqrt{\kappa_{tt}^2 + \kappa_{tn}^2})$$

Derivation of the Asymptotic Form for  $\gg 1$ .

Assume;  $U(v, u) = I(v, u) e^{iku}$

Saddle point at  $v = v'$  for  $v'$  integration.

Let

$$k du = M^2 d\xi \quad \text{where} \quad M = \left(\frac{k}{\kappa g}\right)^{1/3} \gg 1.$$

Reduced Integral Equation

$$I(\xi) = \left[ A_0(\xi) + \frac{A_1}{M(\xi)} + \dots \right] + \int_{-\infty}^{\xi} d\tau I(\tau) \left[ K_0(\xi - \tau) + \frac{K_1(\xi - \tau)}{M} + \dots \right]$$

Let

$$I(\xi) = I_0(\xi) + \frac{I_1(\xi)}{M} + \dots$$

Then

$$I_0(\xi) = A_0(\xi) + \int_{-\infty}^{\xi} d\tau I_0(\tau) K_0(\xi - \tau)$$

and

$$I_1(\xi) = A_1(\xi) + \int_{-\infty}^{\xi} d\tau I_0(\tau) K_1(\xi - \tau) + \int_{-\infty}^{\xi} d\tau I_1(\tau) K_0(\xi - \tau)$$

**B. Vector Problems.**

$$\bar{n} \times \bar{H}(r) = 2 \bar{n} \times \bar{H}_0(r) - \frac{\bar{n}}{2\pi} \times \iint da' \left\{ \bar{n} \times \bar{H}(r') \right\} \times (\bar{r}' - \bar{r}) \frac{1 - ikR}{R^3} e^{ikR}$$

Asymptotic form

$$\hat{n} \times \bar{H}(r) = \bar{I}_0 + \frac{\bar{I}_1}{M} + \dots$$

$$I_0(\xi) = 2e^{-i\frac{\xi^3}{6}} - \frac{e^{-i\frac{\pi}{4}}}{4} \sqrt{\frac{\pi}{2}} \int_{-\infty}^{\xi} d\tau I_0(\tau) (\xi - \tau)^{1/2} e^{-i\frac{(\xi - \tau)^3}{24}}$$

where

$$\bar{I}_0 = \bar{t} I_0$$

**Task 3.1.5 Extension of Paraboloidal Solution to Paraboloidal Surfaces**

A preliminary analysis is being set up to provide theoretically based computations for the surface current on a concave termination such as that typified by the Mk-12 re-entry vehicle. The results of this study will be used for comparison with experimentally obtained measurements in the surface field facility. The investigation has not progressed to a point at which detailed results might be reported.

**Task 3.1.6 Effects of Coating Materials**

Methods for tabulating the Fock functions for a study of the effect of dielectric and ferrite materials on radar cross section are being investigated. The investigation has not progressed to a point at which detailed results might be reported.

**Task 3.1.7 Radar Cross Section of the Cone-Sphere in a Re-entry Environment**

The objective of this task is to compute the back-scattered fields produced by a plane electromagnetic wave incident upon a plasma coated R. V.. The electrical properties of the vehicle will be that associated with either a perfect conductor or an absorber coating. In treating the re-entry sheath, the near wake and the far wake are ignored for present purposes. The near wake may have to be eventually taken into account. This will be especially true for the underdense plasma case when the effects of the rear termination of vehicle have to be taken into account. The present analysis will consider the effects

of the conical portion of the plasma sheath surrounding the vehicle. The fundamental plasma assumption that will be made at present will be the representation of the sheath by a dielectric. This restriction may have to be modified at some later time in considering possible resonance effects taking into account the temperature of the plasma. In addition, fluctuations in the electron density of the plasma sheath characteristic of turbulent flow will be ignored. In the overdense case, these fluctuations produce an electrical effect of a rough or bumpy surface, and may be important when the scale of the associated roughness is the order of, or larger than, the operating wavelength.

Exact expressions of the scattered field are available for a few simple shapes with specified variations in the dielectric properties. Most of the theoretical work on the method of approximation is based on a ray tracing approach. (Jet Propulsion Laboratory, 1965). This method gives a good approximation as long as the conditions for its validity are met. These conditions are not met if the thickness of the dielectric sheath is small compared to the wavelength of the incident wave and/or if the dielectric constant varies appreciatively within a wavelength. Since, according to the data provided by Aerospace Corporation, dielectric sheaths exhibiting the above two properties are of interest, another method for obtaining a solution is needed.

In the past, the method of physical optics has often provided good results for the back scattered fields from a metallic body, whose characteristic dimension is much greater than the wavelength of the incident wave. In this method one assumes that the surface field at a point in the illuminated region is the same as would be induced on an infinite plane occupying the position of the tangent plane, and the surface field in the shadow region is identically zero. A proper integration of these approximate surface field gives the scattered fields in the physical optics approximation.

There are several failures of the physical optics approximation; it doesn't hold in the shadow region, nor on portions of the body where the radii of curvature are small compared to wavelength, nor does it take into account such phenomena as surface or leaky waves that may occur on plasma or dielectric coated bodies. However, in most cases the effects of the shadow portion of the body can be ignored. This will not be true for nose-on incidence to cone-sphere R. V.'s surrounded by an underdense plasma sheath where the rear of the body (the shadow region) has to be taken into account; there the effects of the rear wake will have to be included also. The physical optics method is invalid in the vicinity of the tip of the vehicle. However for metallic bodies, the tip region will appear as the tip region of a conducting cone since here the sheath is extremely thin. It is well known that for nose-on incidence to perfectly conducting cones (where the back-scattered radiation arises from the tip region), the

# SECRET

7741-2-Q

physical optics result yields quite accurate answers. With regard to surface or leaky waves, not predicted by physical optics, some analysis is being carried out to determine when and if they are important.

When the absolute value of dielectric constant is much greater than unity everywhere in the sheath and does not change appreciatively within a wavelength, then the impedance boundary condition holds on the surface of the scattering body (Brekhovskikh, 1960). Uslenghi (1964) derived the physical optics formulas for the scattered fields when the impedance boundary condition is applicable.

First, the general formulas which give the far scattered field in terms of the reflection coefficients of an infinite plane are derived by the method of physical optics. Then, a method for obtaining the reflection coefficients of a metal-backed inhomogeneous dielectric slab is discussed, followed by analysis for a absorber coated body.

## The Generalized Physical Optics Formula for the Back Scattered Fields.

Consider a plane incident electromagnetic wave

$$\vec{E}^{(i)} = \hat{a} e^{i\vec{k} \cdot \vec{r}}$$
$$\vec{H}^{(i)} = \sqrt{\frac{\epsilon_0}{\mu_0}} \hat{b} e^{i\vec{k} \cdot \vec{r}}, \quad (\hat{b} = \hat{k} \times \hat{a})$$

where the symbol,  $\hat{\phantom{a}}$ , indicates a unit vector,  $k = 2\pi/\lambda = \omega \sqrt{\mu_0 \epsilon_0}$  is the wave number in free space and the time dependence factor  $e^{-i\omega t}$  is omitted. By the vector analogue of Green's theorem the scattered field can be expressed in exact form if the total surface fields induced by the incident wave are known exactly (Stratton, 1941):

$$\vec{E}_{\text{exact}}^{(S)}(\mathbf{R}) = \frac{1}{4\pi} \iint_S da \left[ ik \sqrt{\frac{\mu_0}{\epsilon_0}} (\hat{n}(\mathbf{r}) \times \vec{H}(\mathbf{r})) \phi + (\hat{n}(\mathbf{r}) \times \vec{E}(\mathbf{r})) \times \nabla \phi + (\hat{n}(\mathbf{r}) \cdot \vec{E}) \nabla \phi \right] \quad (3.1)$$

where

$$\phi = \frac{e^{ik|\vec{R} - \vec{r}|}}{|\vec{R} - \vec{r}|}$$

and  $\hat{n}$  is a unit normal vector in the outward direction.

In the physical optics approximation for the scattered fields, the total surface fields in the above equation are taken to be the geometrical optics fields in the directly illuminated region and to be zero in the shadow region. The geometrical optics fields over the directly illuminated region are obtained by assuming that at every point the incident field is reflected as though a plane wave were incident on the infinite tangent plane.

Let the incident field in terms of the local geometry be given by:

$$\vec{E}^{(i)} = \hat{a} e^{ik(y \sin \theta - z \cos \theta)} = e^{ik(y \sin \theta - z \cos \theta)} [\sin \gamma \hat{x} + \cos \gamma \cos \theta \hat{y} + \cos \gamma \sin \theta \hat{z}]$$

$$\vec{H}^{(i)} = \sqrt{\frac{\epsilon_0}{\mu_0}} \hat{b} e^{ik(y \sin \theta - z \cos \theta)}, \quad (\hat{b} = \hat{k} \times \hat{a}) \tag{3.2}$$

where the local geometry is shown in Fig. 3-8,

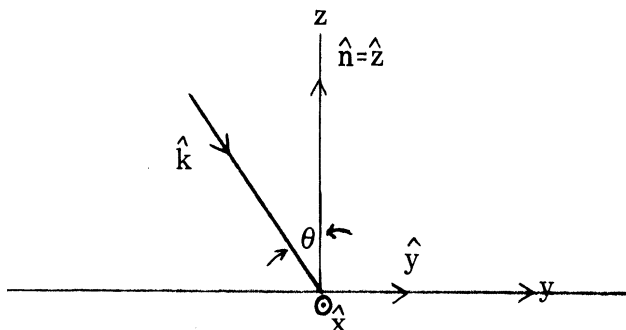


FIG. 3-8: LOCAL CARTESIAN COORDINATE SYSTEM ON THE SURFACE

and  $\gamma = \sin^{-1} [\hat{a} \cdot \hat{x}]$  is the polarization angle. By Snell's law the reflected fields can be expressed in the form:



$$\vec{E}(\mathbf{r}) = e^{ik(y \sin\theta + z \cos\theta)} \left[ \hat{x}\alpha_x + \hat{y}\alpha_y + \hat{z}\alpha_z \right]$$

$$\vec{H}(\mathbf{r}) = \sqrt{\frac{\epsilon_0}{\mu_0}} (\sin\theta \hat{y} + \cos\theta \hat{z}) \times \vec{E}(\mathbf{r}) \quad (3.3)$$

Since  $\vec{E}(\mathbf{r})$ ,  $\vec{H}(\mathbf{r})$  and the propagation direction of the reflected wave are orthogonal to each other, the following relationship holds:

$$\alpha_y \sin\theta + \alpha_z \cos\theta = 0 \quad (3.4)$$

Let us define the reflection coefficients  $R_{\perp}$  and  $R_{\parallel}$  as follows:

$$R_{\perp} \equiv \frac{E_x(\mathbf{r})}{E_x(\mathbf{i})} \quad \text{at the boundary}$$

$$R_{\parallel} \equiv \frac{H_x(\mathbf{r})}{H_x(\mathbf{i})} \quad \text{at the boundary} \quad (3.5)$$

From Eqs. (3.2), (3.3), (3.4) and (3.5) one finds:

$$\alpha_x = R_{\perp} \sin\gamma, \quad \alpha_y = -R_{\parallel} \cos\gamma \cos\theta \quad \text{and} \quad \alpha_z = R_{\parallel} \cos\gamma \sin\theta \quad .$$

So the local geometrical optics field in terms of the reflection coefficients are:

$$\vec{E} = \vec{E}(\mathbf{i}) + \vec{E}(\mathbf{r}) = (1+R_{\perp}) \sin\gamma \hat{x} + (1-R_{\parallel}) \cos\gamma \cos\theta \hat{y} + (1+R_{\parallel}) \cos\gamma \sin\theta \hat{z}$$

$$\vec{H} = \vec{H}(\mathbf{i}) + \vec{H}(\mathbf{r}) = \sqrt{\frac{\epsilon_0}{\mu_0}} \left[ (1+R_{\parallel}) \cos\gamma \hat{x} - (1-R_{\perp}) \sin\gamma \cos\theta \hat{y} - (1+R_{\perp}) \sin\gamma \sin\theta \hat{z} \right]$$

where

$$\hat{z} = \hat{n} , \quad \hat{x} = \frac{\hat{k} \times \hat{n}}{|\hat{k} \times \hat{n}|} , \quad \hat{y} = \frac{\hat{n} \times (\hat{k} \times \hat{n})}{|\hat{k} \times \hat{n}|}$$

$$\cos \theta = -\hat{k} \cdot \hat{n} , \quad \sin \theta = |\hat{k} \times \hat{n}|$$

$$\sin \gamma = \hat{a} \cdot \hat{x} \quad \text{and} \quad \cos \gamma = \hat{k} \times \hat{a} \cdot \hat{x} .$$

Substitution of the above relationships into Eq. (3.1) and integration over only the directly illuminated surface yields the physical optics approximation for the scattered field. In particular, the far back scattered field of a plane electromagnetic wave becomes:

$$\vec{E}^{(S)}(\mathbf{R}) \sim \frac{e^{ikR + i\frac{\pi}{2}}}{\lambda R} [S_1 \hat{a} + S_2 \hat{b}] \quad (3.6)$$

where

$$S_1 = \iint_{\substack{\text{illuminated} \\ \text{region}}} da [\hat{k} \cdot \hat{n}(\vec{r})] \left[ R_{\perp}(\mathbf{r}) - \left\{ R_{\parallel}(\mathbf{r}) + R_{\perp}(\mathbf{r}) \right\} \frac{(\hat{n}(\mathbf{r}) \cdot \hat{a})^2}{[1 - (\hat{n} \cdot \hat{k})^2]} \right] e^{i2\vec{k} \cdot \vec{r}}$$

and

$$S_2 = - \iint_{\substack{\text{illuminated} \\ \text{region}}} da [\hat{k} \cdot \hat{n}(\mathbf{r})] \left[ R_{\parallel}(\mathbf{r}) + R_{\perp}(\mathbf{r}) \right] \frac{[\hat{n}(\mathbf{r}) \cdot \hat{a}][\hat{n}(\mathbf{r}) \cdot \hat{b}]}{[1 - (\hat{n} \cdot \hat{k})^2]} e^{i2\vec{k} \cdot \vec{r}} .$$

When the scattering body is symmetric with respect to the propagation direction  $\hat{k}$  of the incident wave,  $S_2 = 0$  and the back scattered field for a body of revolution is given as:

# SECRET

7741-2-Q

$$\vec{E}(S) \sim \hat{a} \frac{ike^{ikR}}{2R} \int_{\text{illuminated region}} d\rho \rho [-R_{\perp}(z) + R_{\parallel}(z)] e^{i2kz(\rho)} \quad (3.7)$$

where  $z$  is the axis of symmetry of the body,  $\rho = \sqrt{x^2 + y^2}$  is the distance from the axis, and  $z=z(\rho)$  is the equation of the illuminated surface.

For a perfect conductor  $R_{\parallel} = 1$  and  $R_{\perp} = -1$ , and substitution of these relationships into Eq. (3.6) reduces to the well-known result. When the following impedance condition holds (Brekhovskikh, 1960)

$$\vec{E} - (\vec{E} \cdot \hat{n}) \hat{n} = \eta \sqrt{\frac{\mu_0}{\epsilon_0}} \hat{n} \times \vec{H},$$

then the reflection coefficients are given as:

$$R_{\perp} = \frac{\eta(\hat{n} \cdot \hat{k}) + 1}{\eta(\hat{n} \cdot \hat{k}) - 1} \quad \text{and} \quad R_{\parallel} = \frac{(\hat{n} \cdot \hat{k}) + \eta}{(\hat{n} \cdot \hat{k}) - \eta}$$

For a scattering body covered with thin inhomogeneous dielectric sheath, the reflection coefficients may be obtained by the method described in the next section.

### The Reflection Coefficients.

In this section the method of evaluating two reflection coefficients  $R_{\perp}$  and  $R_{\parallel}$  for the metal-backed inhomogeneous dielectric layer is discussed.

The geometry of the situation is shown in Fig. 3-9, where  $h$  is the thickness of the dielectric layer.

The electromagnetic wave equations in inhomogeneous media are:

$$\begin{aligned} \nabla^2 \vec{E} + k^2 \epsilon \vec{E} &= -\nabla(\vec{E} \cdot \frac{\nabla \epsilon}{\epsilon}) \\ \nabla^2 \vec{H} + k^2 \epsilon \vec{H} &= -\frac{\nabla \epsilon}{\epsilon} \times (\nabla \times \vec{H}) \end{aligned} \quad (3.8)$$

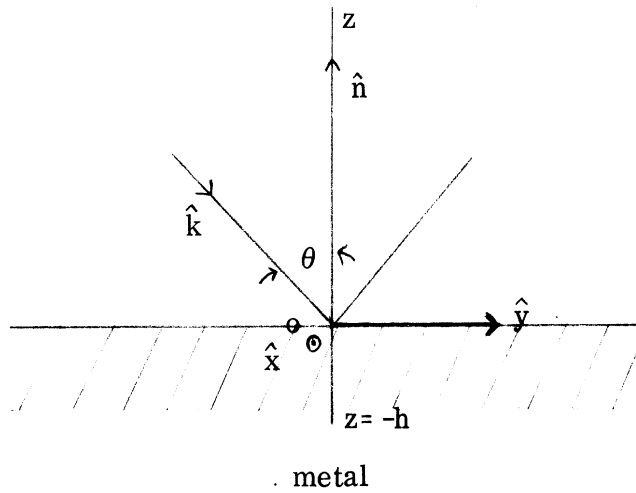


FIG. 3-9: GEOMETRY OF METAL-BACKED DIELECTRIC LAYER.

where  $\epsilon$  is the dielectric constant and  $k = 2\pi/\lambda = \omega \sqrt{\epsilon_0 \mu_0}$  is the wave number in free space.

In the physical optics approximation it is sufficient to assume that the dielectric layer is inhomogeneous only in  $z$  direction.

From the definition of  $R_{\perp}$  and  $R_{\parallel}$  in Eq. (3.5),  $R_{\perp}$  may be evaluated when the electric field vector of the incident plane wave is vertical to the plane of incidence, and  $R_{\parallel}$  when the magnetic field vector is vertical to the plane of incidence. These two different field configurations of the incident wave lead to two different ordinary differential equations.

A. Evaluation of  $R_{\perp}$

When the incident plane wave is vertically polarized,  $\vec{E}^{(i)}$  and  $\vec{H}^i$  are given by Eq. (3.2) with  $\gamma = \pi/2$ . Since  $\epsilon$  is a function of only  $z$  by assumption, the  $\hat{x}$  component of the wave Eq. (3.8) may be written as

$$\frac{\partial^2 E_x}{\partial y^2} + \frac{\partial^2 E_x}{\partial z^2} + k^2 \epsilon(z) E_x = 0 \quad (3.9)$$

Furthermore, due to symmetry of the dielectric layer with respect to  $\hat{y}$  axis and the periodicity of the incident wave, one may write

$$E_x(y, z) \equiv u(z) e^{+iky \sin \theta} .$$

Then Eq. (3.9) is reduced to an ordinary differential equation:

$$\frac{d^2 u}{dz^2} + k^2 [\epsilon(z) - \sin^2 \theta] u = 0 \quad . \quad (3.10)$$

From the boundary conditions that the tangential components of the electric and magnetic fields are continuous at  $z=0$  and the tangential component of electric field is zero at  $z=-h$ , one finds

$$\begin{aligned} u &= 0 \quad \text{at} \quad z = -h \\ E_x^{(i)} + E_x^{(r)} &= u \quad \text{at} \quad z = 0 \\ -ik \cos \theta (E^{(i)} - E^{(r)}) &= \frac{du}{dz} \quad \text{at} \quad z = 0 \end{aligned} \quad (3.11)$$

The solution of Eq. (3.10) under the boundary conditions in Eq. (3.11) gives the reflection coefficient  $R_{\perp}$

$$R_{\perp} = \frac{\cos \theta u(z=0) - \frac{i}{k} \frac{du}{dz}(z=0)}{\cos \theta u(z=0) + \frac{i}{k} \frac{du}{dz}(z=0)}$$

### B. Evaluation of $R_{\parallel}$

When the magnetic field vector of the incident plane wave is vertical to the plane of incidence, the expression of the incident electromagnetic wave is given by Eq. (3.2) with  $\gamma=0$ :

$$\bar{H}^{(i)} = \sqrt{\frac{\epsilon_0}{\mu_0}} \hat{x} e^{ik(y \sin \theta - z \cos \theta)} .$$

Substituting the relationship

$$H_x(y, z) = v(z) e^{iky \sin \theta}$$

the wave Eq. ( 3.8 ) in dielectric layer becomes

$$\frac{d^2 v}{dz^2} - \frac{1}{\epsilon} \frac{d\epsilon}{dz} \frac{dv}{dz} + k^2 [\epsilon(z) - \sin^2 \theta] v = 0 .$$

The required boundary conditions are:

$$\begin{aligned} \frac{dv}{dz} &= 0 \quad \text{at} \quad z = -h \\ H_x^{(i)} + H_x^{(r)} &= v \quad \text{at} \quad z = 0 \\ - ik \cos \theta [H_x^{(i)} - H_x^{(r)}] &= \frac{1}{\epsilon(0_-)} \frac{dv}{dz} \quad \text{at} \quad z = 0 \end{aligned} \tag{3.12}$$

where  $\epsilon(0_-)$  is the dielectric constant of the layer at the interface of the dielectric layer and free space.

The reflection coefficient  $R_{||}$  is:

$$R_{||} = \frac{\cos \theta v(z=0) - \frac{i}{\epsilon(0_-)k} \frac{dv}{dz}(z=0)}{\cos \theta v(z=0) + \frac{i}{\epsilon(0_-)k} \frac{dv}{dz}(z=0)} .$$

For an arbitrary  $\epsilon(z)$ , the two boundary value problems for  $R_{||}$  and  $R_{\perp}$  can, at least, always be solved by the numerical method (Swift and Evans, 1963).

# SECRET

7741-2-Q

## Application to Absorber Coated Bodies.

The above results can be easily applied to absorber coated bodies, for magnetic type of absorbers which can be characterized by an impedance boundary condition (Weston, 1963)

$$\underline{E} - (\underline{E} \cdot \underline{n})\underline{n} = \eta \sqrt{\frac{\mu_0}{\epsilon_0}} \underline{n} \times \underline{H} \quad .$$

This will hold provided that the index of refraction of the absorber material is sufficiently large.

The only change in computing the reflection coefficients is in the boundary conditions. In place of the first equation of set of Eqs. (3.11), the following must be used:

$$ku = i\eta \frac{\partial u}{\partial z} \quad \text{at } z = -h \quad ,$$

and, in place of the first equation of the set of equations given by (3.12), the following must be used:

$$\frac{\partial v}{\partial z} = -ik\eta \left(\frac{\epsilon}{\epsilon_0}\right) v \quad \text{at } z = -h \quad .$$

## Calculations.

The back-scattering cross section is being considered for a  $11^\circ$  half-angle cone surrounded by a plasma sheath typical of various altitudes and velocities. Profiles of the plasma at a distance 13 inches along the cone have been given by Aerospace for seven different cases, together with the appropriate scaling laws. For each case, the number of collisions per second is given, along with the plasma profile in terms of a table giving the electron density versus distance from the surface. For clarification of the present and future analysis, the different cases are given a profile number as follows:

<u>Profile No.</u>	<u>Altitude</u>	<u>Comments</u>	<u>Type of Flow</u>
1	200 K ft	Clean air	Laminar
2	150 K ft	Clean air	Laminar
3	150 K ft	Contaminated air	Laminar
4	100 K ft		Turbulent
5	80 K ft		Turbulent
6	60 K ft		Turbulent
7	30 K ft		Turbulent

# SECRET

7741-2-Q

The first step was to obtain the equivalent relative dielectric constant  $\epsilon'$  from the values of the electron density  $N_e$  and number of collisions per second from the relation

$$\epsilon' = \alpha + i\beta = 1 + \frac{\left[-1 + i\frac{\nu}{2\pi f}\right]}{\left(\frac{f}{f_p}\right)^2 + \left(\frac{\nu}{2\pi f_p}\right)^2},$$

for the following operating frequencies  $f = 100$  MHz, 500 MHz, 1 KMHz, 5 KMHz, 10 KMHz. The plasma frequency  $f_p$  is given in terms of  $N_e$  by the following

$$f_p = 8979 \sqrt{N_e}$$

These calculations gave some immediate results on the effect of the sheath on the back-scattering. For the above range of frequencies the relative permittivity of profiles 1 and 2 were so close to unity, that it can be concluded that the effect of the sheath is negligible in these cases. For profile 3, the same result holds for the upper two operating frequencies 5 KMHz and 10 KMHz.

The profiles of the real and imaginary parts ( $\alpha$  and  $\beta$ , respectively) are presented for the remaining cases in Figs. 3-10 through 3-19 for a distance 13 inches from the tip of the cone.

The next step is to compute the reflection coefficients for various stations along the surface. This is being undertaken at the present time.

When these values are obtained, Eqs. (3.6) and (3.7) will be used to compute the back-scattered field. However, the process of integration has to be performed analytically. From the numerical results, expressions for the amplitude and phase of the reflection coefficients will be found as a function of distance along the conical surface. Then, stationary phase or similar techniques will be used to evaluate the integral. This is important to insure that the contribution is from the tip for nose-on scattering and to enable one to give the results a physical interpretation. If the range of integration was made finite, the upper limit of integration would yield a term to the back-scattered cross-section which would correspond to a finite conical sheath, which does not correspond to the physical situation. The sheath extends well beyond the vehicle and for the extremely overdense case the effect of the vehicle termination is negligible.



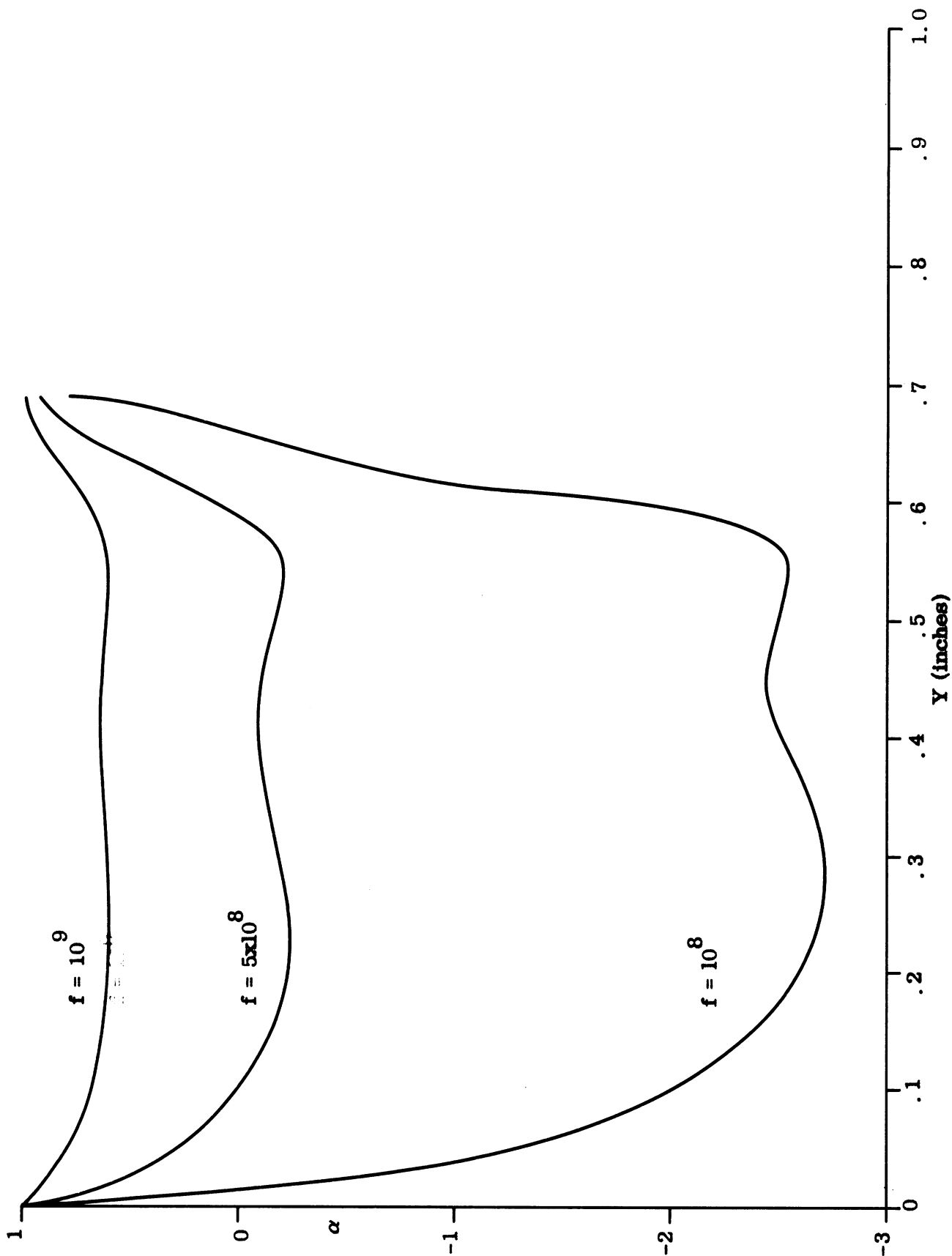


FIG. 3-10: REAL PART OF RELATIVE DIELECTRIC CONSTANT FOR SHEATH OF PROFILE 3.

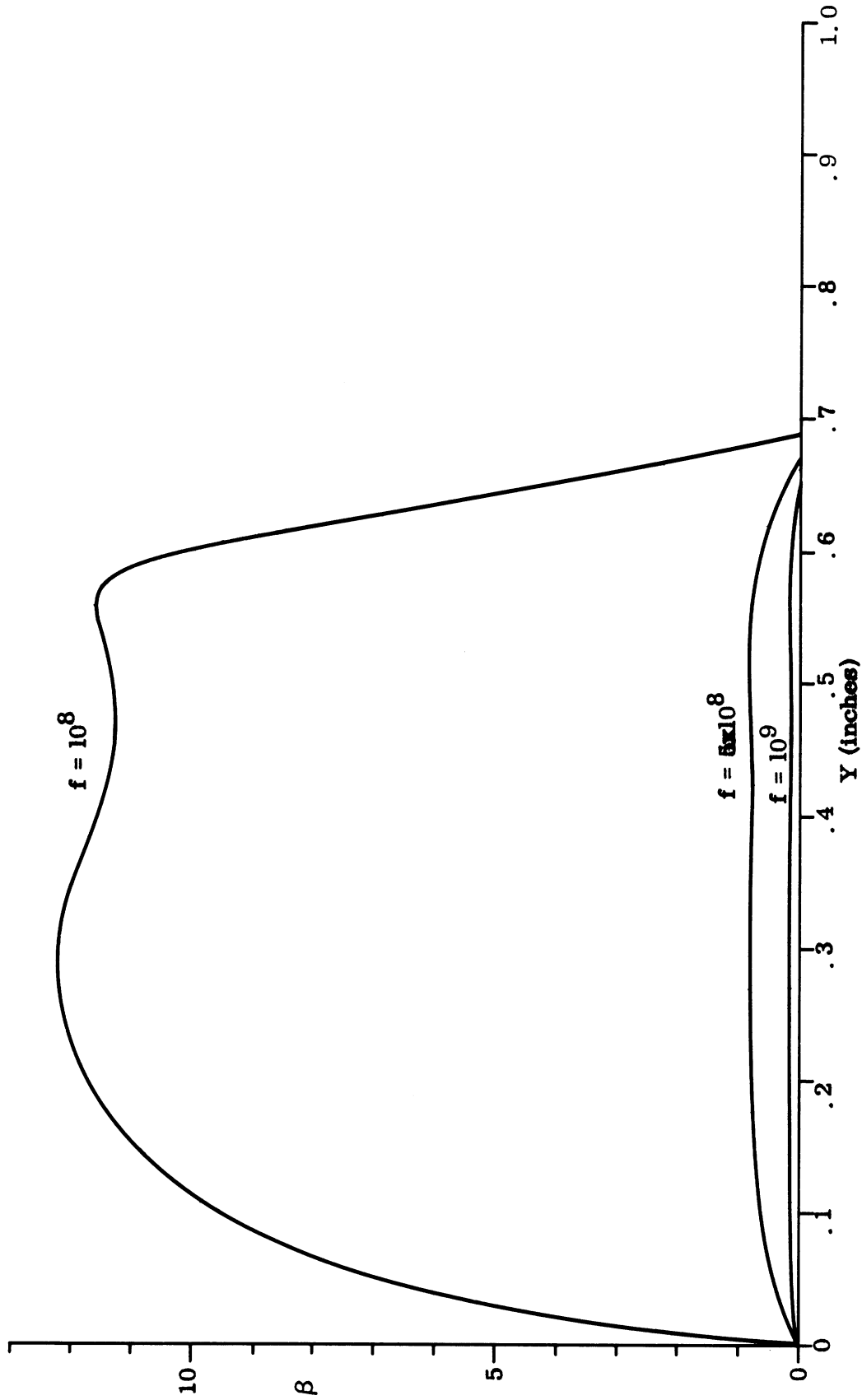


FIG. 3-11: IMAGINARY PART OF RELATIVE DIELECTRIC CONSTANT FOR SHEATH OF PROFILE 3.

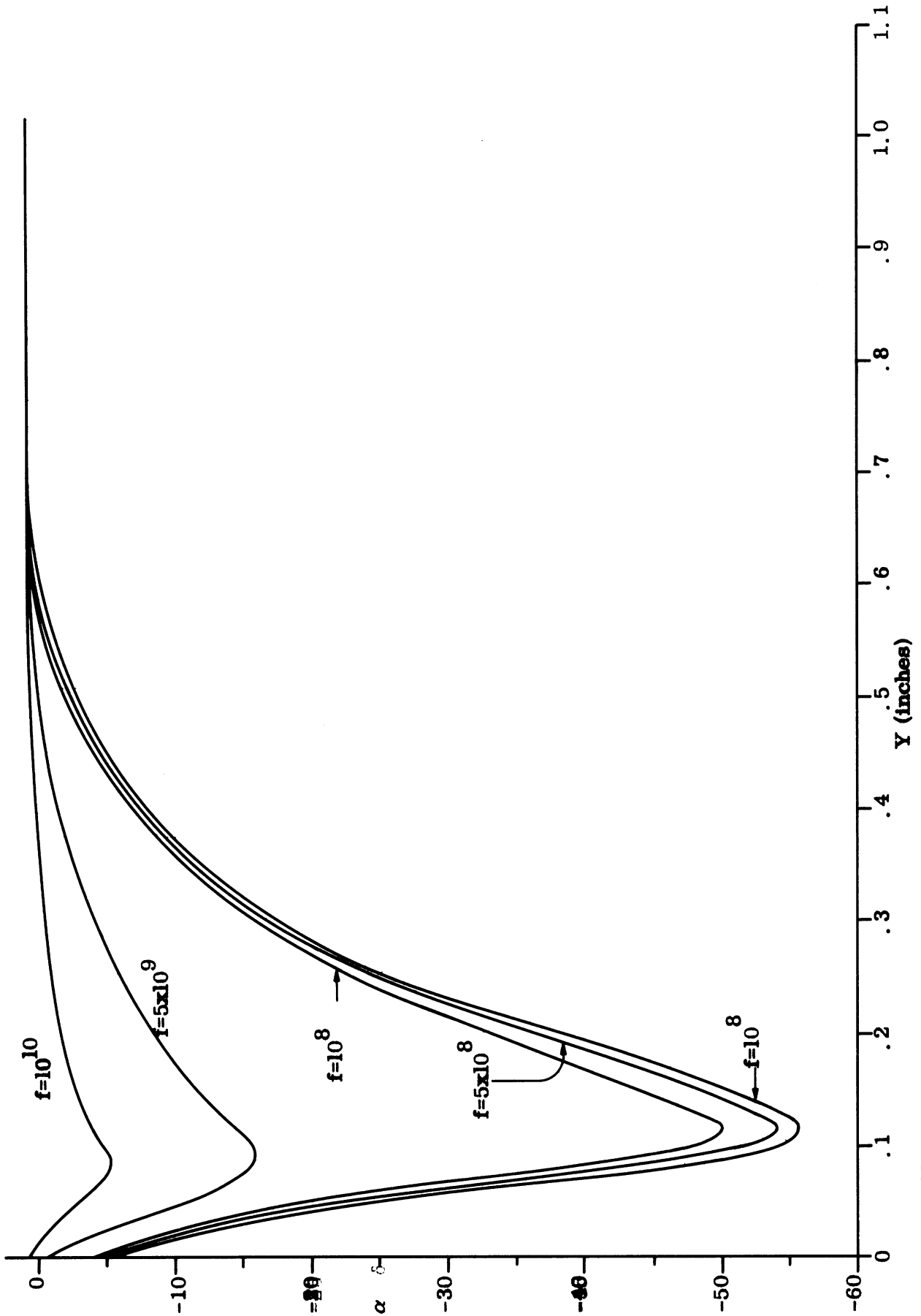


FIG. 3-12: REAL PART OF RELATIVE DIELECTRIC CONSTANT FOR SHEATH OF PROFILE 4.

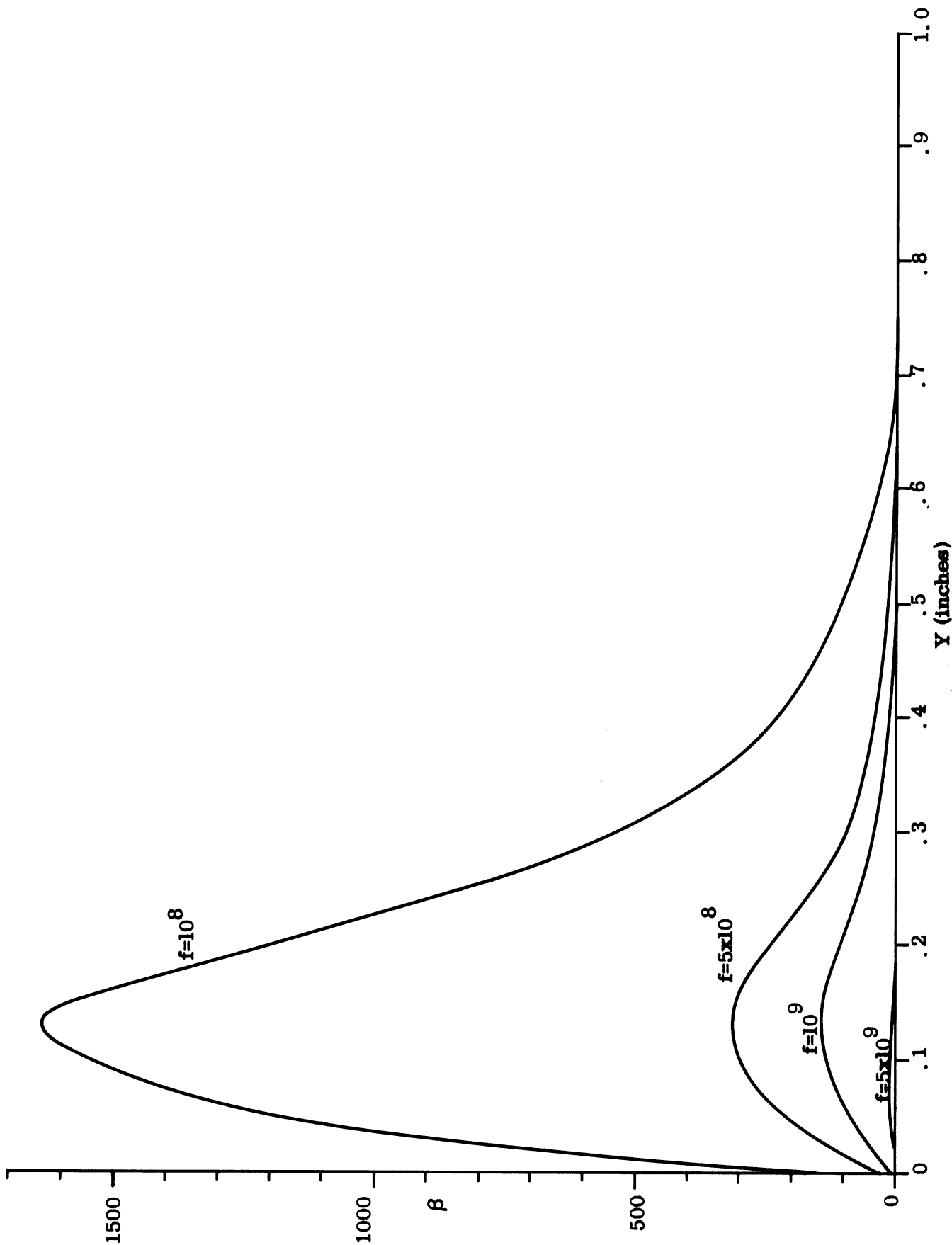


FIG. 3-13: IMAGINARY PART OF RELATIVE DIELECTRIC CONSTANT FOR SHEATH OF PROFILE 4.

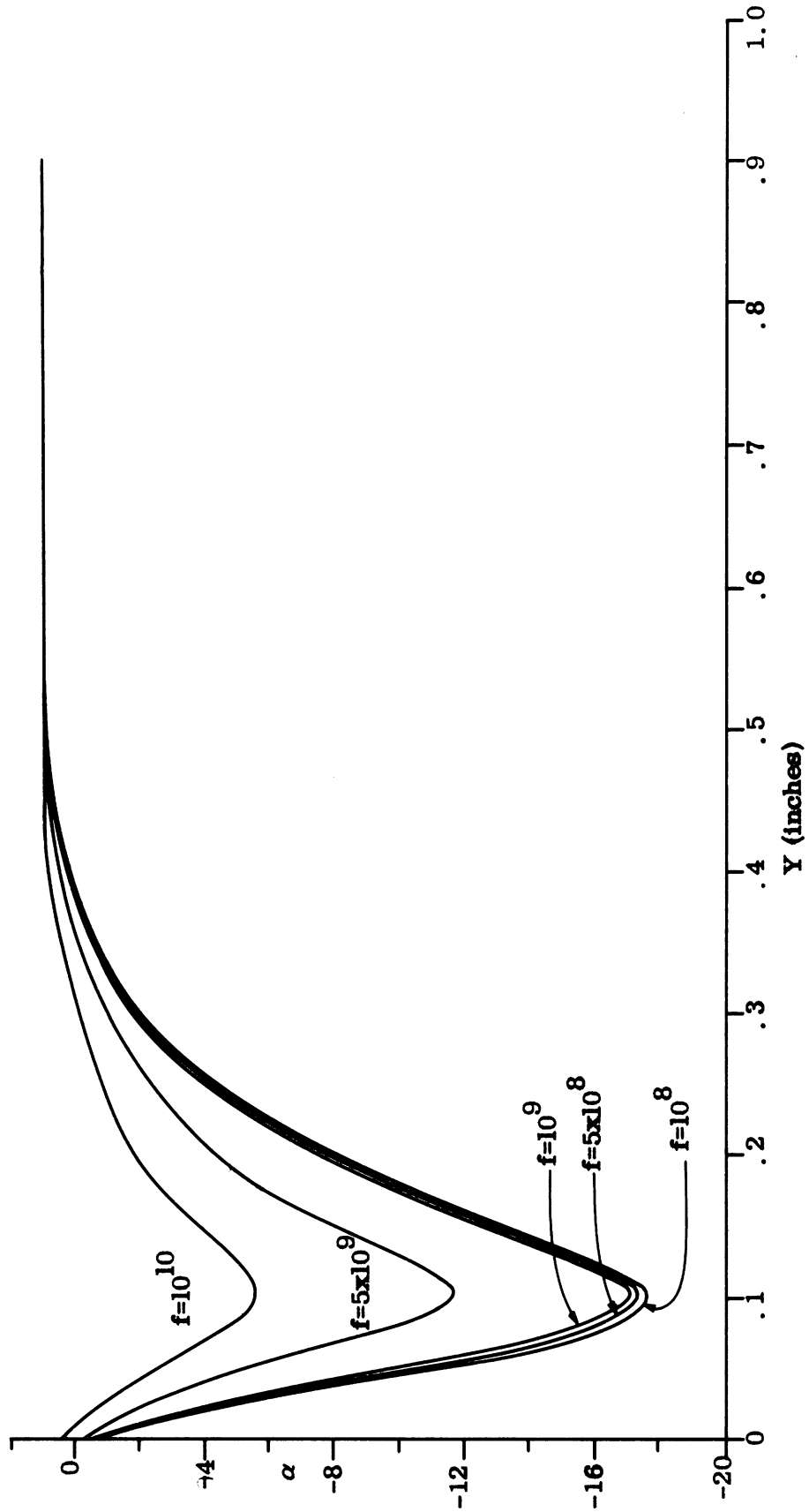


FIG. 3-14: REAL PART OF RELATIVE DIELECTRIC CONSTANT FOR SHEATH OF PROFILE 5.

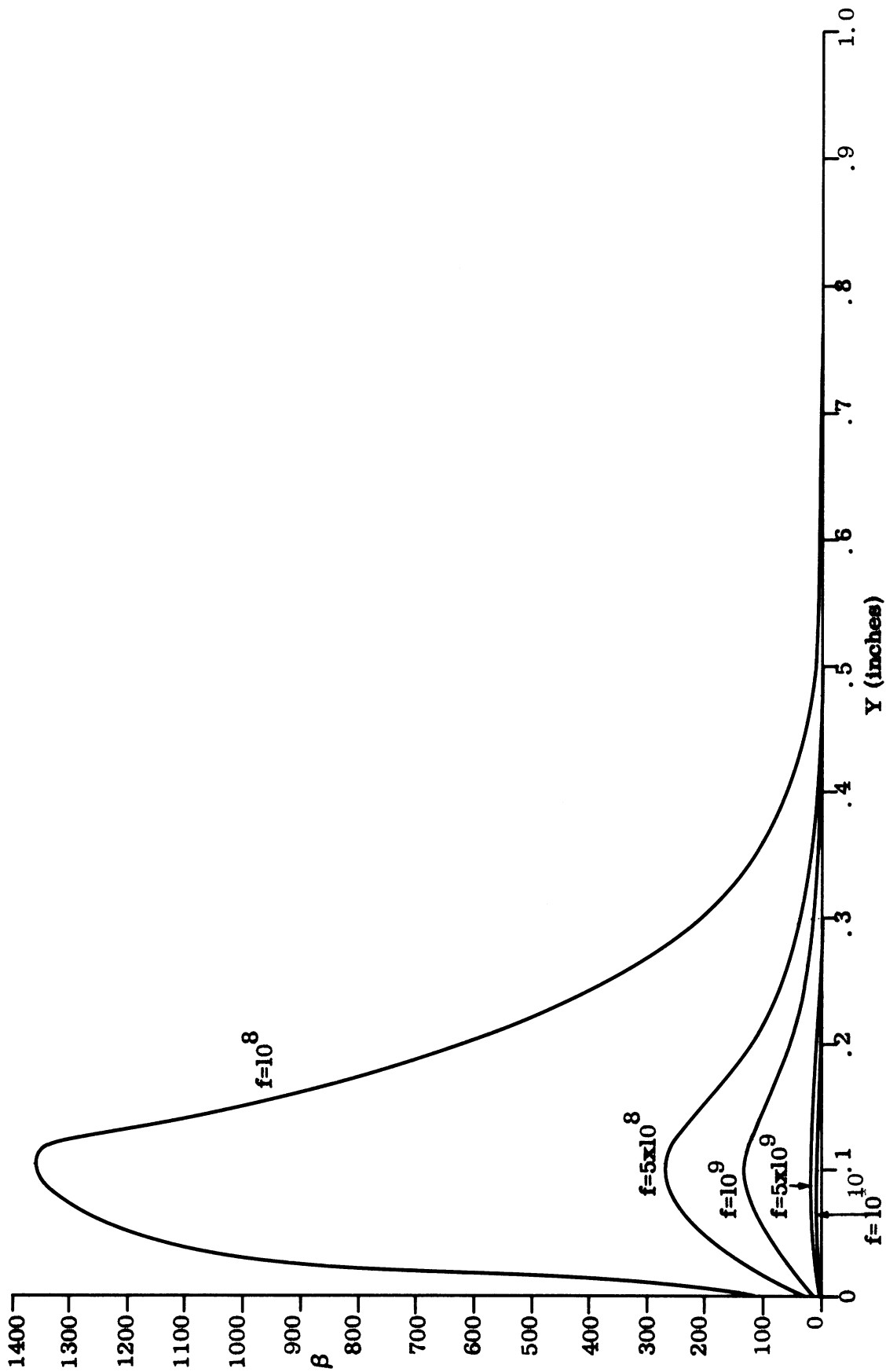


FIG. 3-15: IMAGINARY PART OF RELATIVE DIELECTRIC CONSTANT FOR SHEATH OF PROFILE 5.

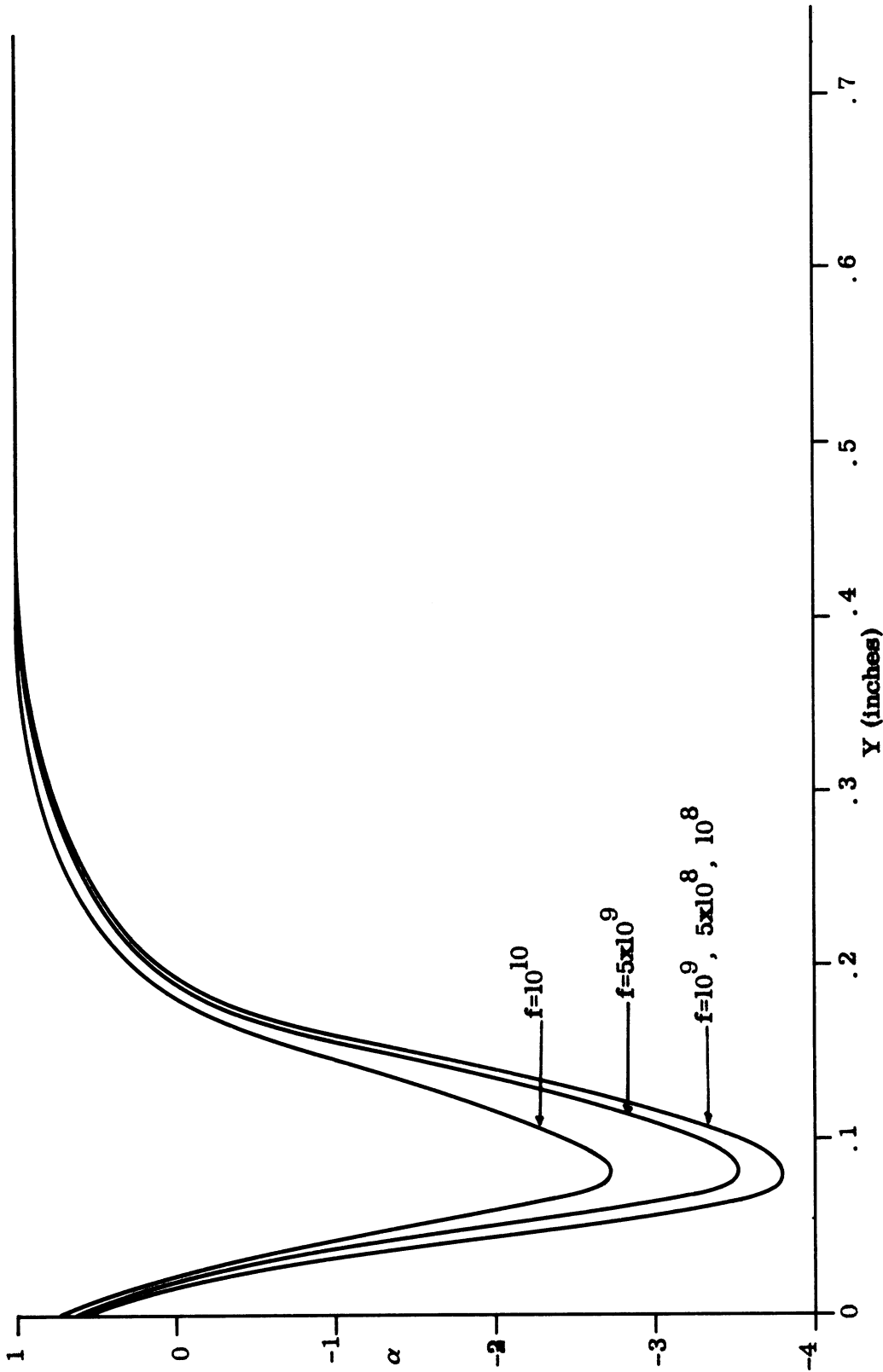


FIG. 3-16: REAL PART OF RELATIVE DIELECTRIC CONSTANT FOR SHEATH OF PROFILE 6.

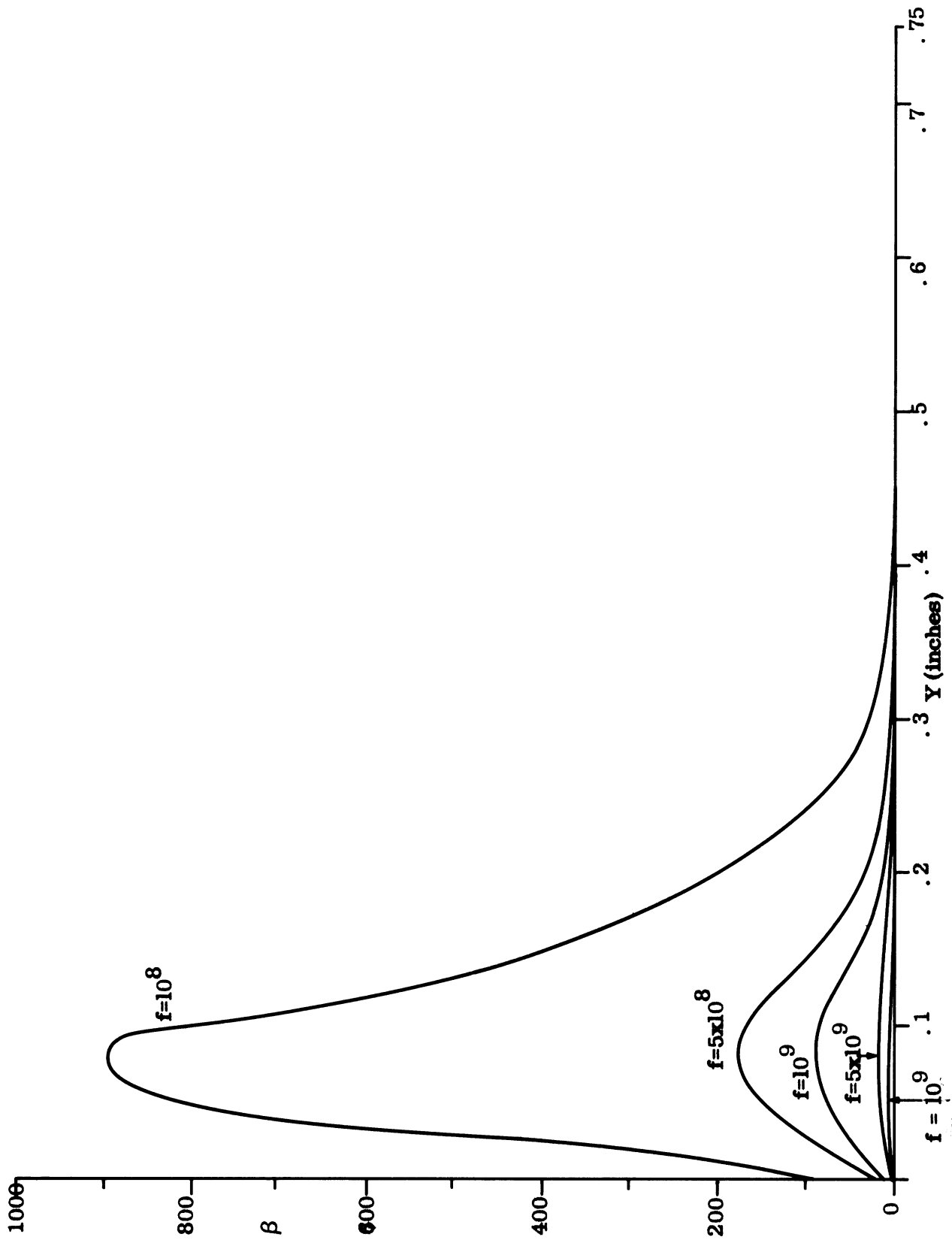


FIG. 3-17: IMAGINARY PART OF RELATIVE DIELECTRIC CONSTANT FOR SHEATH OF PROFILE 6.



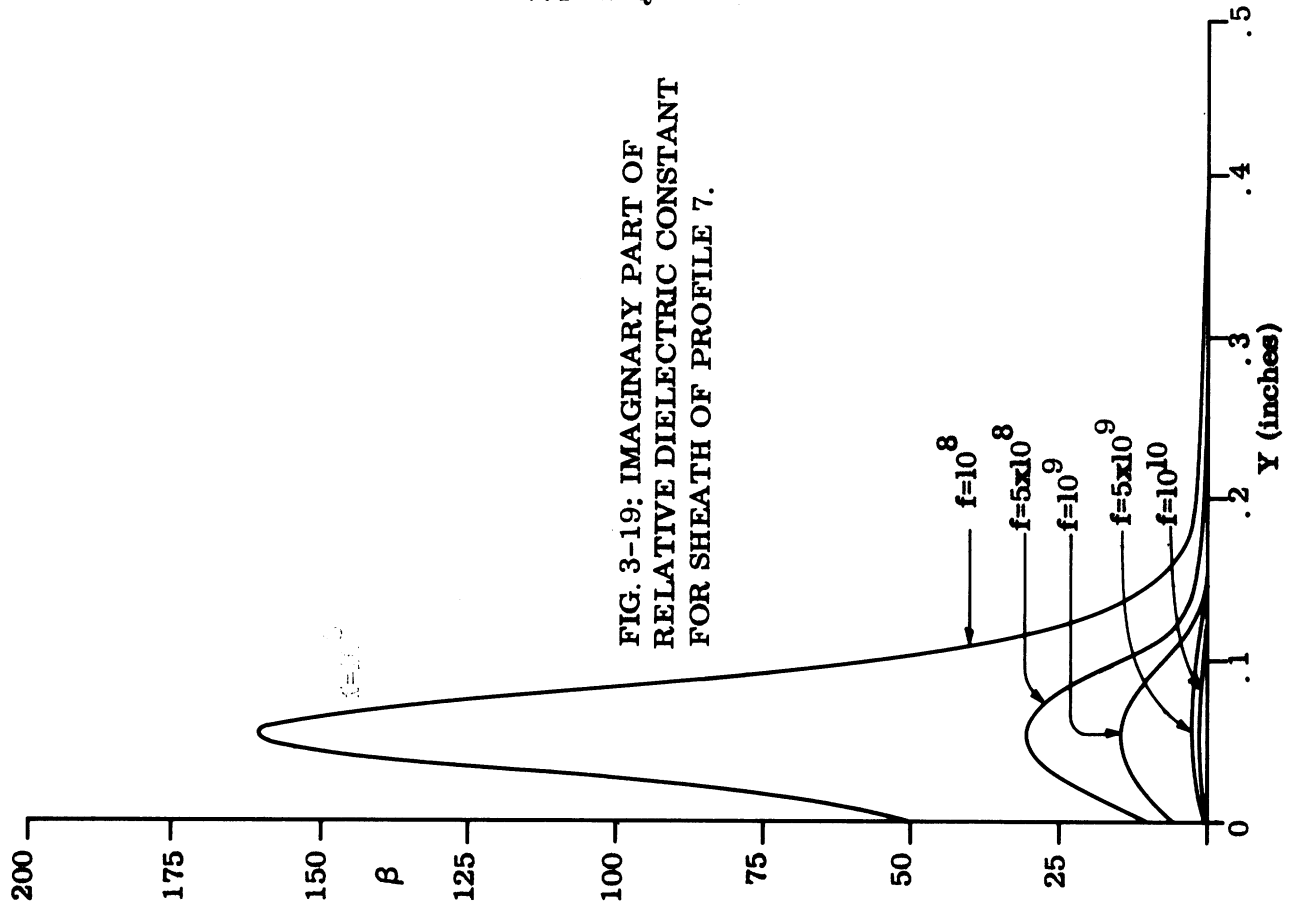


FIG. 3-19: IMAGINARY PART OF RELATIVE DIELECTRIC CONSTANT FOR SHEATH OF PROFILE 7.

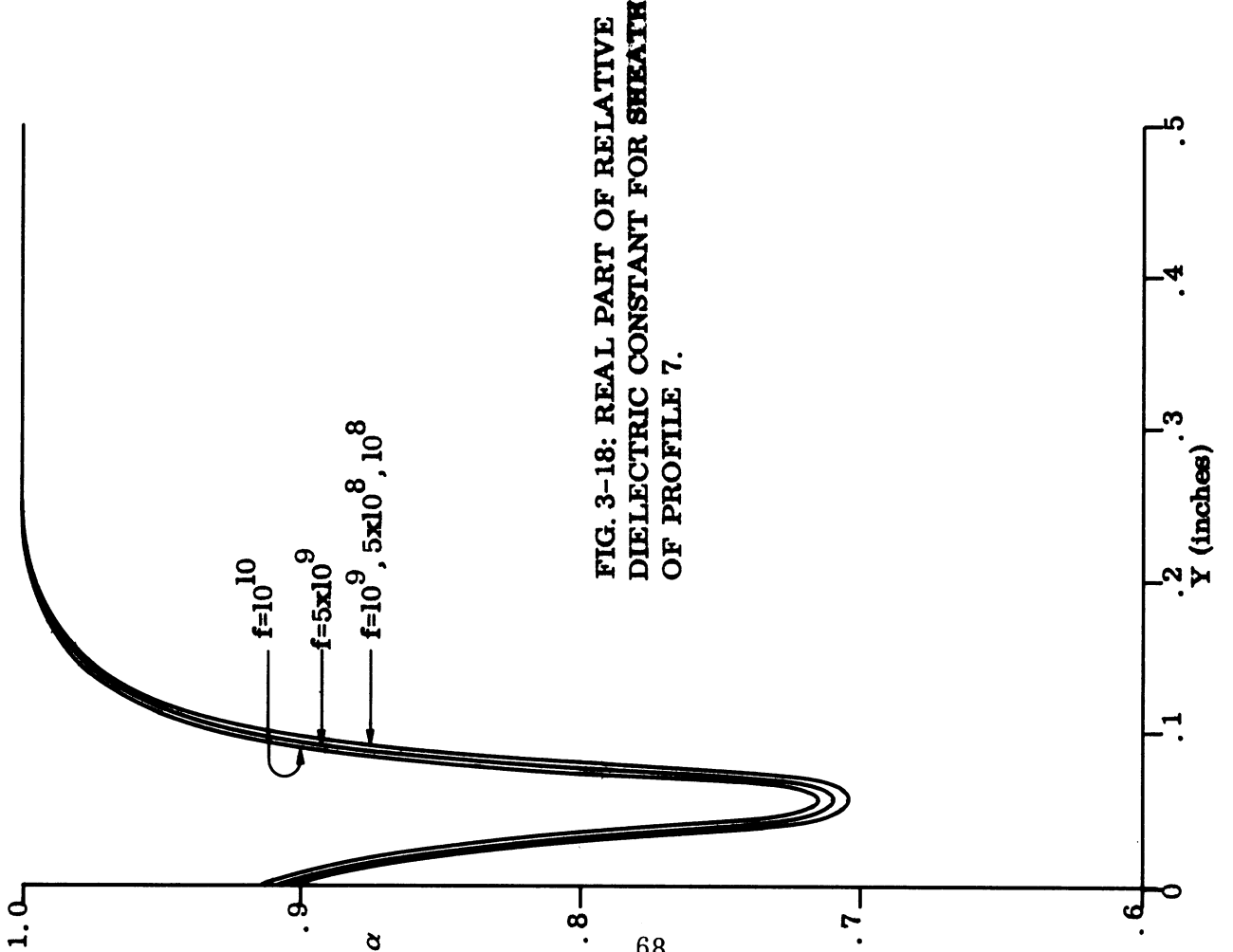


FIG. 3-18: REAL PART OF RELATIVE DIELECTRIC CONSTANT FOR SHEATH OF PROFILE 7.

# SECRET

7741-2-Q

## REFERENCES

- AVCO Corporation, "Radar Cross Section and Radar Cross Section Reduction Studies of the Cone Sphere," Technical Report RAD-TR-66-3, March 1966  
SECRET.
- Brekhovskikh, Leonid M. (1960) Waves in Layered Media, (Academic Press, New York).
- Goodrich, R. F., E. Ar, B.A.Harrison, S.Hong, T.B.A.Senior and S.E.Stone (1965) "Radar Cross Section of the Metallic Cone-Sphere--Final Report," The University of Michigan Radiation Laboratory Report No. 7030-5-T. SECRET
- "Interaction of Spacecraft and Other Moving Bodies with Natural Plasma," (1965), Literature Search No. 541, Jet Propulsion Lab., Cal. Inst. Tech., pp. 34-62.
- Knott, E. F. (1965) "Design and Operation of a Surface Field Measurement Facility," The University of Michigan Radiation Laboratory Report 7030-7-T.
- Meixner, J. and F.W. Schafke (1954) Mathieu'sche Funktionen und Sphäroidfunktionen, (Springer-Verlag, Berlin).
- Schultz, F.V. (1950) "Scattering by a Prolate Spheroid," The University of Michigan Willow Run Research Center, Report No. UMM-42.
- Stratton, J.A. (1941) Electromagnetic Theory, (McGraw-Hill, New York).
- Swift, C. T. and J.S. Evans (1963) "Generalized Treatment of Plane Electromagnetic Waves Passing Through an Isotropic Inhomogeneous Plasma Slab at Arbitrary Angles of Incidence," NASA Tech. Report TR-R-172.
- Uslenghi, P. (1964) "Radar Cross Section of Imperfectly Conducting Bodies at Small Wavelengths," Alta Frequenza, XXXIII, No. 8, 541-546.
- Weston, V.H. (1963) "Theory of Absorbers in Scattering," IEEE Trans., , AP-11, No. 5, 578-584.
- Wigner, E. (1931) Gruppentheorie, (F. Vieweg and Sons, Brunschweig)

SECRET

Security Classification

SECRET

## DOCUMENT CONTROL DATA - R&amp;D

(Security classification of title, body of abstract and indexing annotation must be entered when the overall report is classified)

1. ORIGINATING ACTIVITY (Corporate author) The University of Michigan Radiation Laboratory Department of Electrical Engineering		2a. REPORT SECURITY CLASSIFICATION SECRET	
		2b. GROUP 4	
3. REPORT TITLE Investigation of Re-entry Vehicle Surface Fields Quarterly Report No. 2			
4. DESCRIPTIVE NOTES (Type of report and inclusive dates) Quarterly Report No. 2 18 March - 18 June 1966			
5. AUTHOR(S) (Last name, first name, initial) Goodrich, Raymond F.; Harrison, Burton A.; Knott, Eugene F.; Weston, Vaughan H.			
6. REPORT DATE June 1966		7a. TOTAL NO. OF PAGES 69	7b. NO. OF REFS 12
8a. CONTRACT OR GRANT NO. AF 04(694)-834		8a. ORIGINATOR'S REPORT NUMBER(S) 7741-2-Q	
b. PROJECT NO.		8b. OTHER REPORT NO(S) (Any other numbers that may be assigned this report) BSD-TR-66-255	
c.			
d.			
10. AVAILABILITY/LIMITATION NOTICES In addition to security requirements which apply to this document, and must be met, this document is subject to special export controls and each transmittal to foreign governments or foreign nationals may be made only with prior approval of BSD (BSYDF), Norton AFB, Calif. 92409.			
11. SUPPLEMENTARY NOTES		12. SPONSORING MILITARY ACTIVITY Ballistic Systems Division Deputy for Ballistic Missile Re-entry Systems Air Force Systems Command, Norton AFB, Calif.	
13. ABSTRACT (S) This is the Second Quarterly Report on Contract No. AF 04(694)-834 and covers the period 18 March to 18 June 1966. Progress on the SURF program is discussed. This program has as its objective the determination of the radar cross section of cone-sphere shaped re-entry vehicles by means of a study of the fields induced on the surface of vehicle models by incident radar energy. During this reporting period, some experimental difficulties involving the design of probes to measure tangential electric fields were resolved. Measurements were made of the electromagnetic properties of coating materials to be used in the study. Work on the theoretical basis for the prediction of the radar cross sections continued. Computations involving the re-entry environment are discussed.			

DD FORM 1473  
1 JAN 64

SECRET

SECRET  
Security Classification

14. KEY WORDS	LINK A		LINK B		LINK C	
	ROLE	WT	ROLE	WT	ROLE	WT
Radar cross section Cone-sphere-like objects Surface fields Electromagnetic probes Experimental data Re-entry vehicles Coating materials Re-entry environment						

INSTRUCTIONS

1. **ORIGINATING ACTIVITY:** Enter the name and address of the contractor, subcontractor, grantee, Department of Defense activity or other organization (*corporate author*) issuing the report.
- 2a. **REPORT SECURITY CLASSIFICATION:** Enter the overall security classification of the report. Indicate whether "Restricted Data" is included. Marking is to be in accordance with appropriate security regulations.
- 2b. **GROUP:** Automatic downgrading is specified in DoD Directive 5200.10 and Armed Forces Industrial Manual. Enter the group number. Also, when applicable, show that optional markings have been used for Group 3 and Group 4 as authorized.
3. **REPORT TITLE:** Enter the complete report title in all capital letters. Titles in all cases should be unclassified. If a meaningful title cannot be selected without classification, show title classification in all capitals in parenthesis immediately following the title.
4. **DESCRIPTIVE NOTES:** If appropriate, enter the type of report, e.g., interim, progress, summary, annual, or final. Give the inclusive dates when a specific reporting period is covered.
5. **AUTHOR(S):** Enter the name(s) of author(s) as shown on or in the report. Enter last name, first name, middle initial. If military, show rank and branch of service. The name of the principal author is an absolute minimum requirement.
6. **REPORT DATE:** Enter the date of the report as day, month, year, or month, year. If more than one date appears on the report, use date of publication.
- 7a. **TOTAL NUMBER OF PAGES:** The total page count should follow normal pagination procedures, i.e., enter the number of pages containing information.
- 7b. **NUMBER OF REFERENCES:** Enter the total number of references cited in the report.
- 8a. **CONTRACT OR GRANT NUMBER:** If appropriate, enter the applicable number of the contract or grant under which the report was written.
- 8b, 8c, & 8d. **PROJECT NUMBER:** Enter the appropriate military department identification, such as project number, subproject number, system numbers, task number, etc.
- 9a. **ORIGINATOR'S REPORT NUMBER(S):** Enter the official report number by which the document will be identified and controlled by the originating activity. This number must be unique to this report.
- 9b. **OTHER REPORT NUMBER(S):** If the report has been assigned any other report numbers (*either by the originator or by the sponsor*), also enter this number(s).
10. **AVAILABILITY/LIMITATION NOTICES:** Enter any limitations on further dissemination of the report, other than those

imposed by security classification, using standard statements such as:

- (1) "Qualified requesters may obtain copies of this report from DDC."
- (2) "Foreign announcement and dissemination of this report by DDC is not authorized."
- (3) "U. S. Government agencies may obtain copies of this report directly from DDC. Other qualified DDC users shall request through \_\_\_\_\_."
- (4) "U. S. military agencies may obtain copies of this report directly from DDC. Other qualified users shall request through \_\_\_\_\_."
- (5) "All distribution of this report is controlled. Qualified DDC users shall request through \_\_\_\_\_."

If the report has been furnished to the Office of Technical Services, Department of Commerce, for sale to the public, indicate this fact and enter the price, if known.

11. **SUPPLEMENTARY NOTES:** Use for additional explanatory notes.
12. **SPONSORING MILITARY ACTIVITY:** Enter the name of the departmental project office or laboratory sponsoring (*paying for*) the research and development. Include address.
13. **ABSTRACT:** Enter an abstract giving a brief and factual summary of the document indicative of the report, even though it may also appear elsewhere in the body of the technical report. If additional space is required, a continuation sheet shall be attached.

It is highly desirable that the abstract of classified reports be unclassified. Each paragraph of the abstract shall end with an indication of the military security classification of the information in the paragraph, represented as (TS), (S), (C), or (U).

There is no limitation on the length of the abstract. However, the suggested length is from 150 to 225 words.

14. **KEY WORDS:** Key words are technically meaningful terms or short phrases that characterize a report and may be used as index entries for cataloging the report. Key words must be selected so that no security classification is required. Identifiers, such as equipment model designation, trade name, military project code name, geographic location, may be used as key words but will be followed by an indication of technical context. The assignment of links, rules, and weights is optional.